Polycarbon Ligand Complexes: Synthesis, Molecular Structures, and Selected EHMO Studies of Ru_4, Ru_5, and Ru_6 Clusters with Carbon Ligands Derived from Phosphinodiynes

Peter Blenkiron,[†,‡] Gary D. Enright,[†] Paul J. Low,[†] John F. Corrigan,[‡] Nicholas J. Taylor,[‡] Yun Chi,[§] Jean-Yves Saillard,*[,||] and Arthur J. Carty*[,†,‡]

Steacie Institute for Molecular Sciences, National Research Council of Canada, 100 Sussex Drive, Ottawa, Ontario, Canada K1A OR6, Guelph-Waterloo Centre for Graduate Work in Chemistry, Waterloo Campus, Department of Chemistry, University of Waterloo, Waterloo, Ontario, Canada, N2L 3G1, Department of Chemistry, National Tsing Hua University, Hsinchu 30043, Taiwan, and Laboratoire de Chimie du Solide et Inorganique Moléculaire UMR-CNRS 6511, Université de Rennes 1, 35042 Rennes, Cedex, France

Received January 29, 1998

Thermolysis of the monosubstituted cluster $Ru_3(CO)_{11}(Ph_2PC{\equiv}C{-}C{\equiv}CR)$ (R = Bu^t, Ph, $SiMe_3$), obtained via CO substitution in $Ru_3(CO)_{12}$, results in P−C and Ru−Ru bond cleavage. Recombination of the fragments yields a range of polyruthenium compounds containing $-(C{\equiv}C)-_n$ ligands (n = 2−4). The complexes $Ru_4(CO)_9(\mu\text{-}PPh_2)_2\{\mu_4\text{-}\eta^1,\eta^2,\eta^2,\eta^1\text{-}C{\equiv}C{-}C{=}C\text{-}(Bu^t){-}C{\equiv}C{-}C{\equiv}CBu^t\}$ (**2**), $Ru_4(CO)_{10}(\mu\text{-}CO)(\mu_4\text{-}PPh)\{\mu_4\text{-}\eta^1,\eta^1,\eta^2,\eta^2\text{-}(Bu^tC{\equiv}C)C{\equiv}CPh\}$ (**3**), $Ru_4(CO)_{10}(\mu_4\text{-}PPh)(\mu_4\text{-}\eta^1,\eta^1,\eta^3,\eta^3\text{-}PhC{\equiv}C{-}C{\equiv}CBu^t)$ (**4**), $Ru_5(CO)_{11}(\mu\text{-}CO)(\mu\text{-}PPh_2)_2(\mu_3\text{-}\eta^1,\eta^1,\eta^1\text{-}C{\equiv}C{-}C{\equiv}CBu^t)(\mu_4\text{-}C)(\mu_2\text{-}\eta^1,\eta^1\text{-}C{-}C{\equiv}CBu^t)$ (**5**), $Ru_6(CO)_{13}(\mu\text{-}CO)_2(\mu\text{-}PPh_2)(\mu_5\text{-}C)(\mu_3\text{-}\eta^1,\eta^1,\eta^1\text{-}C{-}C{\equiv}CR)$ (**6a**, R = Bu^t; **6b**, R = Ph), and $\{Ru_2(CO)_6(\mu\text{-}PPh_2\}_2(\mu\text{-}\eta^1,\eta^2{:}\mu\text{-}\eta^1,\eta^2\text{-}C{\equiv}C{-}C{\equiv}C{-})$ (**7**) have been fully characterized. The crystal structure of **2** revealed a polyunsaturated C_8 chain formed by the head−tail coupling of two diynyl units bound to the metal core in μ_4-η^3 mode to produce a pendant penta-1-enediyne functionality. Clusters **3** and **4** feature square-planar arrangements of metal atoms capped on one side by a μ_4-PPh ligand and on the other side by a $-C{\equiv}C{-}C{\equiv}C-$ group. The hydrocarbyl units in **3** and **4** arise as a result of phenyl migration from a PPh_2 group to a terminal carbon of the diynyl fragment. On heating, **3** readily decarbonylates to generate **4**. The pentanuclear cluster **5** and hexanuclear cluster **6** both contain unusually coordinated C_4 chains which may be considered as being comprised of carbido- and alkynyl-substituted alkylidyne ligands. The alkylidyne carbide ligand is coordinated across the basal face of a pentagonal pyramid in **6** and across a distorted spiked square in **5**. The latter also features a second C_4 group which forms a rare μ_3-η^1-butadiynyl ligand. An EHMO analysis of the model compound $Ru_6(CO)_{13}(\mu\text{-}CO)_2(\mu\text{-}PH_2)(\mu_5\text{-}C)(\mu_3\text{-}\eta^1,\eta^1,\eta^1\text{-}C{-}C{\equiv}CH)$ (**6a′**) suggests that the cluster is best described in terms of an Ru_4C_2 octahedron bicapped by a phosphido-bridged Ru_2 unit, with the C−C−R (R = C≡CH) radical contributing a total of seven electrons to the CVE count of the entire polyhedron.

Introduction

Ynyl (−C≡C−R) and polyynyl [$-(C{\equiv}C)_n-$R] ligands are potential building blocks for new classes of organometallic molecules with interesting structural and materials properties.[1] For example, rod-shaped complexes exhibiting liquid crystalline and nonlinear optical properties have been constructed by linking metal centers via $M-C_{sp}$ bonds and the extended π-systems in polyynyl ligands.[2] Models for molecular wires with chains of sp-hybridized carbon capped by metal fragments $[ML_n]-C_x-[ML_n]$ have also been designed.[3] In these carbon-rich complexes, the π-electrons of the ynyl functionality are not directly involved in metal coordination. However, simple ynyl groups −C≡CR are

(1) (a) Bruce, M. I.; Ke, M.; Low, P. J. *Chem. Commun.* **1996**, 2405. (b) Irwin, M. J.; Jia, G.; Payne, N. C.; Puddephatt, R. J. *Organometallics* **1996**, *15*, 51. (c) Khan, M. S.; Kakkar, A. K.; Ingham, S. L.; Raithby, P. R.; Lewis, J.; Spencer, B.; Wittman, F.; Friend, R. H. *J. Organomet. Chem.* **1994**, *472*, 247. (d) Stang, P. J.; Tykwinski, R. *J. Am. Chem. Soc.* **1992**, *114*, 4411. (e) Sun, Y.; Taylor, N. J.; Carty, A. J. *Organometallics* **1992**, *11*, 4293. (f) Brady, M.; Weng, W.; Gladysz, J. A. *J. Chem. Soc., Chem. Commun.* **1994**, 2655. (g) Lang, H. *Angew. Chem., Int. Ed. Engl.* **1994**, *33*, 547. (h) Fyfe, H. B.; Mlekuz, M.; Zargarin, D.; Taylor, N. J.; Marder, T. B. *J. Chem. Soc., Chem. Commun.* **1991**, 188. (i) Koutsantonis, G. A.; Selegue, J. P. *J. Am. Chem. Soc.* **1991**, *113*, 2316. (j) Berenguer, J. R.; Forniés, J.; Lalinde, E.; Martínez, F. *Organometallics* **1995**, *14*, 2532. (k) Esteruelas, M. A.; Oro, L. A.; Schrickel, J. *Organometallics* **1997**, *16*, 796. (l) Werner, H.; Gevert, O.; Haquette, P. *Organometallics* **1997**, *16*, 803. (m) Yam, Y. W.-W.; Lau, V. C.-Y.; Cheung, K.-K. *Organometallics* **1996**, *15*, 1740.

(2) (a) Rourke, J. P.; Bruce, D. W.; Marder, T. B. *J. Chem. Soc., Dalton Trans.* **1995**, 317. (b) Marder, T. B.; Lesley, G.; Yuan, Z.; Fyfe, H. B.; Chow, P.; Stringer, G.; Jobe, I. R.; Taylor, N. J.; Williams, I. D.; Kurtz, S. K. *ACS Symp. Ser.* **1991**, *455*, 605. (c) Lewis, J.; Khan, M. S.; Kakkar, A. K.; Johnson, B. F. G.; Marder, T. B.; Fyfe, H. B.; Wittmann, F.; Friend, R. H.; Dray, A. E. *J. Organomet. Chem.* **1992**, *425*, 165. (d) Calabrese, J. C.; Cheng, L. T.; Green, J. C.; Marder, S. R.; Tam, W. *J. Am. Chem. Soc.* **1991**, *113*, 7227. (e) Zhou, Y.; Seyler, J. W.; Weng, W.; Arif, A. M.; Gladysz, J. A. *J. Am. Chem. Soc.* **1993**, *115*, 8509. (f) Lavastre, O.; Plass, J.; Bachmann, P.; Guesmi, S.; Moinet, C.; Dixneuf, P. H. *Organometallics* **1997**, *16*, 184.

S0276-7333(98)00059-4 CCC: $15.00
Publication on Web 05/13/1998

known to be versatile π-ligands, and many examples of polymetallic complexes bearing these fragments are known.[4] Butadiynyl ($-C\equiv C-C\equiv CR$) and higher ynyl ligands should, therefore, be powerful agents for the assembly of metal cluster complexes containing polycarbon ligands.

Detailed studies of both mono- and bis-phosphino-substituted alkynes and diynes $R_2PC\equiv CR'$,[5] $R_2PC\equiv CPR'_2$,[6] and $R_2PC\equiv C-C\equiv CPR'_2$[7] have shown that these ligands are excellent sources of metal-coordinated ynyl fragments. In an earlier report, we described the synthesis and characterization of the series of binuclear $\sigma-\pi$ butadiynyl complexes $Ru_2(CO)_6$ (μ-PPh_2)(μ-η^1,η^2-$C\equiv C-C\equiv CR$) (**1a**, R = Bu^t; **1b**, R = Ph; **1c**, R = $SiMe_3$), which were obtained from the thermolysis of the diynyl phosphine clusters $Ru_3(CO)_{11}(Ph_2PC\equiv C-C\equiv CR)$.[8] In

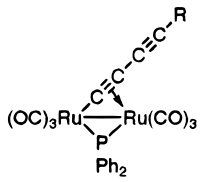

R = Bu^t (**1a**), Ph (**1b**), $SiMe_3$ (**1c**)

addition to **1**, several higher nuclearity clusters containing unusual polyyne ligands were also produced. These unsaturated C_nR ligands are coordinated on Ru_4, Ru_5, and Ru_6 cluster frameworks as μ_3-butadiynyl, μ_4-butadiyne, μ_4-butadiynediyl, μ_4-vinyldiyneynyl, and μ_5 and μ_6-alkylidyne carbide groups. In this paper, we describe the generation of these polyunsaturated C_4- and C_8-containing species derived via oxidative $P-C_{sp}$ bond cleavage and, in some cases, C−C coupling. The nature of the R group has a significant bearing on the products formed. Thus, while pyrolysis of $Ru_3(CO)_{11}(Ph_2PC\equiv C-C\equiv CBu^t)$ gave **1a** and the clusters $Ru_4(CO)_9$(μ-PPh_2)$_2${μ_4-η^1,η^2,η^2,η^1-$C\equiv C-C=C(Bu^t)-C\equiv C-C\equiv CBu^t$} (**2**), $Ru_4(CO)_{10}$(μ-CO)(μ_4-PPh){μ_4-η^1,η^1, η^2,η^2-$(Bu^tC\equiv C)C\equiv C$-Ph} (**3**), $Ru_4(CO)_{10}$(μ_4-PPh)(μ_4-η^1,η^1,η^3,η^3-$PhC\equiv C-C\equiv C$-Bu^t) (**4**), $Ru_5(CO)_{11}$(μ-CO)(μ-PPh_2)$_2$(μ_3-η^1,η^1,η^1-$C\equiv C-C\equiv CBu^t$)(μ_4-C)(μ_2-η^1,η^1-$C-C\equiv CBu^t$) (**5**), and $Ru_6(CO)_{13}$-(μ-CO)$_2$(μ-PPh_2)(μ_5-C)(μ_3-η^1,η^1,η^1-$C-C\equiv CBu^t$) (**6a**), similar reactions of $Ru_3(CO)_{11}(Ph_2PC\equiv C-C\equiv CPh)$ yielded only **1b** and **6b** while in the case of $Ru_3(CO)_{11}(Ph_2$-$PC\equiv C-C\equiv CSiMe_3)$ the complexes **1c** and {$Ru_2(CO)_6$-(μ-PPh_2}$_2$(μ-η^1,η^2:μ-η^1,η^2-$C\equiv C-C\equiv C-$) (**7**) were the only isolable products obtained.

The clusters **2**, **3**, **4**, **5**, **6a**, and **7** illustrate some of the diverse bonding modes polyacetylenic fragments may adopt in different metal and electronic environments. An analysis of the electron counting together with EHMO calculations on the unusual cluster **6** have provided insights into the bonding within the Ru_6C_2 framework. A preliminary account of part of this work has been published.[9]

Results and Discussion

(i) Synthesis, Structure, and Spectroscopy. (a) Thermolysis of $Ru_3(CO)_{11}(Ph_2PC\equiv CC\equiv CBu^t)$. A solution of $Ru_3(CO)_{11}(Ph_2PC\equiv C-C\equiv CBu^t)$ in refluxing THF darkens to a color near black over a 4 h period. Chromatographic separation of the product mixture gave, in order of elution, trace amounts of $Ru_3(CO)_{12}$, yellow $Ru_2(CO)_6$(μ-PPh_2)(μ-η^1,η^2-$C\equiv C-C\equiv CBu^t$) (**1a**, 31%), orange $Ru_4(CO)_{10}$(μ_4-PPh)(μ_4-η^1,η^1,η^3,η^3-$PhC\equiv C-C\equiv CBu^t$) (**4**, 3%), red-brown $Ru_6(CO)_{13}$(μ-$CO)_2$(μ-PPh_2)-(μ_5-C)(μ_3-η^1,η^1,η^1-$C-C\equiv CBu^t$) (**6a**, 3%), an orange band containing $Ru_4(CO)_{10}$(μ-CO)(μ_4-PPh){μ_4-η^1,η^1,η^2,η^2-$(Bu^tC\equiv C)C\equiv CPh$} (**3**, 1%) and $Ru_5(CO)_{11}$(μ-CO)(μ-PPh_2)$_2$-(μ_3-η^1,η^1,η^1-$C\equiv C-C\equiv CBu^t$)(μ_4-C)(μ_2-η^1,η^1-$C-C\equiv CBu^t$) (**5**, 5%), and finally a green-blue band of $Ru_4(CO)_9$(μ-PPh_2)$_2$-{μ_4-η^1,η^2,η^2,η^1-$C\equiv C-C=C(Bu^t)-C\equiv C-C\equiv CBu^t$} (**2**, 12%). The clusters are numbered in a way that facilitates a discussion of their chemistry. The structures of clusters **1**−**6** were unambiguously established by single-crystal X-ray crystallography and supported by ^{1}H, ^{13}C, and ^{31}P NMR and IR spectroscopies as well as FAB mass spectroscopy in some cases. These compounds are essentially air-stable in the solid state, have varying degrees of stability in solution, and, with the exception of the hexanuclear cluster **6a**, are all soluble in hexane.

Complex **2** readily crystallized from a rich turquoise-colored band. The presence of two Bu^t groups was apparent from ^{1}H NMR spectroscopy (singlets at δ 1.13 and 1.19), while integration of the resonances in the aromatic region suggested the presence of four Ph groups. The ^{31}P NMR spectrum exhibited a single resonance at δ 209.2, which is consistent with the presence of a μ_2-phosphido ligand. This singlet was maintained even at temperatures as low as 183 K. The

(3) (a) Coat, F.; Lapinte, C. *Organometallics* **1996**, *15*, 477. (b) Seyler, J. W.; Weng, W.; Zhou, Y.; Gladysz, J. A. *Organometallics* **1993**, *12*, 3802. (c) Le Narvor, N.; Toupet, L.; Lapinte, C. *J. Am. Chem. Soc.* **1995**, *117*, 7129. (d) Weng, W.; Bartik, T.; Brady, M.; Bartik, B.; Ramsden, J. A.; Arif, A. M.; Gladysz, J. A. *J. Am. Chem. Soc.* **1995**, *117*, 11922. (e) Rappert, T.; Nürnberg, O.; Werner, H.; *Organometallics* **1993**, *12*, 1359. (f) Le Narvor, N.; Lapinte, C. *Organometallics* **1995**, *14*, 634. (g) Falloon, S. B.; Arif, A. M.; Gladysz, J. A. *Chem. Commun.* **1997**, 630. (h) Gevert, O.; Wolf, J.; Werner, H. *Organometallics* **1996**, *15*, 2806. (i) Bruce, M. I.; Denisovich, L. I.; Low, P. J.; Peregudova, S. M.; Ustynyuk, N. A. *Mendeleev Commun.* **1996**, 200. (j) Akita, A.; Chung, M.-C.; Sakurai, A.; Sugimoto, S.; Terada, M.; Tanaka, M.; Moro-oka, Y. *Organometallics* **1997**, *16*, 4882.

(4) (a) Carty, A. J. *Pure Appl. Chem.* **1982**, *54*, 113. (b) Sappa, E.; Tiripicchio, A.; Braunstein, P. *Coord. Chem. Rev.* **1985**, *65*, 219. (c) Sappa, E.; Tiripicchio, A.; Braunstein, P. *Chem. Rev.* **1983**, *83*, 203. (d) Nast, R. *Coord. Chem. Rev.* **1982**, *47*, 89. (e) Cherkas, A. A.; Doherty, S.; Cleroux, M.; Hogarth, G.; Randall, L. H.; Breckenridge, S. M.; Taylor, N. J.; Carty, A. J. *Organometallics* **1992**, *11*, 1701 and references therein. (f) Akita, M.; Moro-oka, Y. *Bull. Chem. Soc. Jpn.* **1995**, *68*, 420.

(5) See, for example: (a) Patel, H. A; Fischer, R. G; Carty, A. J.; Naik, D. V.; Palenik, G. J. *J. Organomet. Chem.* **1973**, *60*, C49. (b) Carty, A. J.; Dymock, K.; Paik, H. N.; Palenik, G. J. *J. Organomet. Chem.* **1974**, *70*, C17. (c) Cherkas, A. A.; Randall, L. H.; MacLaughlin, S. A.; Mott, G. N.; Taylor, N. J.; Carty, A. J. *Organometallics* **1988**, *7*, 969. (d) Nucciarone, D.; MacLaughlin, S. A.; Taylor, N. J.; Carty, A. J. *Organometallics* **1988**, *7*, 106. (e) Cherkas, A. A.; Taylor, N. J.; Carty, A. J. *J. Chem. Soc., Chem. Commun.* **1990**, 385. (f) MacLaughlin, S. A.; Taylor, N. J.; Carty, A. J. *Organometallics* **1983**, *2*, 1194. (g) Van Gastel, F.; MacLaughlin, S. A.; Lynch, M.; Carty, A. J.; Sappa, E.; Tiripicchio, A.; Tiripicchio-Camellini, M. *J. Organomet. Chem.* **1987**, *326*, C65.

(6) (a) Carty, A. J.; Efraty, A.; Ng, T. W.; Birchall, T. *Inorg. Chem.* **1970**, *9*, 1263. (b) Bruce, M. I.; Williams, M. L.; Patrick, J. M.; White, A. H. *J. Chem. Soc., Dalton Trans.* **1985**, 1229. (c) Bruce, M. I.; Snow, M. R.; Tiekink, E. R. T.; Williams, M. L. *J. Chem. Soc., Chem. Commun.* **1986**, 701. (d) Daran, J. C.; Jeannin, Y.; Kristiansson, O. *Organometallics* **1985**, *4*, 882. (e) Adams, C. J.; Bruce, M. I.; Skelton, B. W.; White, A. H. *J. Organomet. Chem.* **1992**, *423*, 97.

(7) (a) Adams, C. J.; Bruce, M. I.; Horn, E.; Skelton, B. W.; Tiekink, E. R. T.; White, A. H. *J. Chem. Soc., Dalton Trans.* **1993**, 3299. (b) *Ibid*. **1993**, 3313. (c) Adams, C. J.; Bruce, M. I.; Skelton, B. W.; White, A. H. *J. Organomet. Chem.* **1993**, *450*, C9.

(8) Blenkiron, P.; Corrigan, J. F.; Pilette, D.; Taylor, N. J.; Carty, A. J. *Can. J. Chem.* **1996**, *74*, 2349.

(9) Blenkiron, P.; Taylor, N. J.; Carty, A. J. *J. Chem. Soc., Chem. Commun.* **1995**, 327.

Table 1. Crystallographic Data for Clusters 2−7

	2	3	4	5	6a	7
formula	$C_{49}H_{38}O_9P_2Ru_4$	$C_{31}H_{19}O_{11}PRu_4$	$C_{30}H_{19}O_{10}PRu_4$	$C_{52}H_{38}O_{12}P_2Ru_5$	$C_{35}H_{19}O_{15}PRu_6 0.5C_4H_{10}O$	$C_{40}H_{20}O_{12}P_2Ru_4$
fw	1237.1	1002.7	974.7	1422.1	1354.0	1158.8
cryst size (mm)	0.03 × 0.05 × 0.15	0.30 × 0.22 × 0.22	0.36 × 0.26 × 0.24	0.10 × 0.30 × 0.45	0.154 × 0.318 × 0.144	0.03 × 0.08 × 0.25
cryst syst	orthorhombic	monoclinic	triclinic	triclinic	triclinic	monoclinic
space group	$Pc2_1n$	$P2_1/c$	$P\bar{1}$	$P\bar{1}$	$P\bar{1}$	$P2/c$
a, Å	9.4560(11)	9.214(2)	10.542(1)	12.556(2)	12.588(2)	13.625(15)
b, Å	15.1600(15)	39.171(6)	11.508(2)	15.365(2)	13.391(3)	11.188(12)
c, Å	34.495(4)	9.639(3)	14.450(2)	15.548(2)	13.923(5)	13.897(16)
α, deg			96.77(1)	75.45(2)	78.05(2)	
β, deg		102.36(2)	100.33(1)	89.59(2)	68.56(2)	105.100(10)
γ, deg			105.71(1)	68.29(2)	83.84(2)	
V, Å^3	4944.96(3)	3398.5(13)	1634.3(4)	2685.1(7)	2135.8(9)	2045.27(3)
Z	4	4	2	2	2	2
D_c, g cm^{-3}	1.622	1.960	1.981	1.759	2.105	1.882
radiation	Mo Kα	Mo Kα	Mo Kα	Mo Kα	Mo Kα	Mo Kα
diffractometer	Siemens SMART CCD	Siemens R3m/V	Siemens R3m/V	Siemens R3m/V	Siemens R3m/V	Siemens SMART CCD
temp, K	173	200	200	294	200	173
F(000)	2418.81	1936	940	1392	1298	1114.92
μ, cm^{-3}	12.9	18.47	19.15	14.92	21.72	15.9
scan type	*ω*	*ω*	*ω*	*ω*	*ω*	*ω*
2*θ* range, deg	3.0−48.0	4.0−45.0	4.0−56.0	4.0−50.0	4.0−50.0	3.0−57.5
no. of rflns measd	18 720	4455	7925	9505	7900	13 945
no. of unique rflns	6397	4455	7925	9505	7558	5272
no. of obsd rflns	6271 ($I > 2.5\sigma(I)$)	3597 ($F > 6.0\sigma(F)$)	6622 ($F > 6.0\sigma(F)$)	7756 ($F > 6.0\sigma(F)$)	6434 ($F > 6.0\sigma(F)$)	3812 ($I > 2.5\ \sigma(I)$)
no. of params refined	372	444	426	668	579	244
final *R*, R_w	0.078, 0.108	0.0247, 0.0290	0.0219, 0.0268	0.0240, 0.0292	0.0207, 0.0264	0.061, 0.069
GOF	5.08	2.01	2.18	1.97	1.82	2.62
max, min resd density, e Å^{-3}	+ 2.29, −2.22	+ 0.35, −0.33	+ 0.46, −0.45	+ 0.45, −0.30	+ 0.61, −0.37	+ 1.13, −1.16

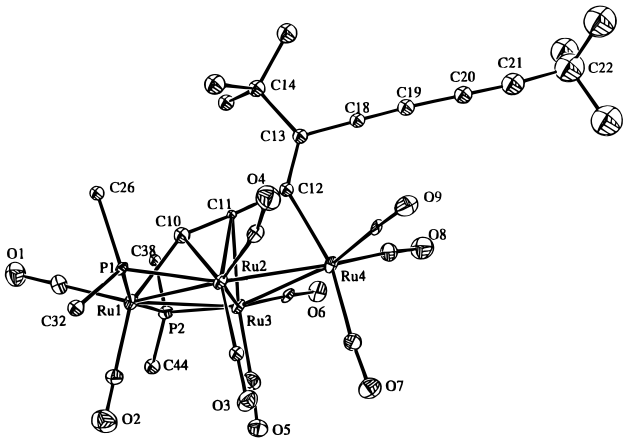

Figure 1. Molecular structure and numbering scheme for **2**. Only the *ipso*-carbons of the phenyl groups are shown, and hydrogen atoms have been omitted for clarity.

structure of **2** was determined by a single-crystal X-ray diffraction analysis, and a molecule is shown in Figure 1. Selected bond distances and angles are given in Table 2.

Cluster **2**, $Ru_4(CO)_9(\mu\text{-}PPh_2)_2\{\mu_4\text{-}\eta^1,\eta^2,\eta^2,\eta^1\text{-}C{\equiv}C{-}C{=}C(Bu^t)\text{-}C{\equiv}C{-}C{\equiv}CBu^t\}$ consists of a tetranuclear metal core exhibiting an open flat butterfly geometry.

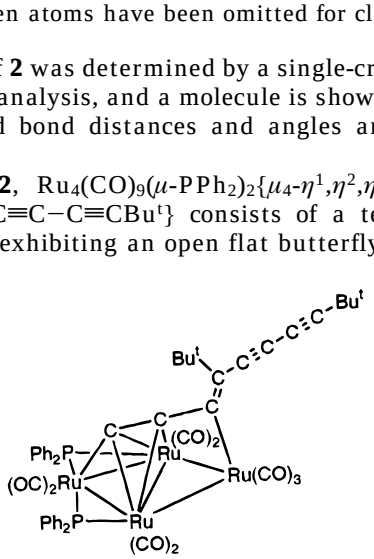

2

Table 2. Selected Bond Distances (Å) and Angles (deg) for Cluster 2

Ru(1)−Ru(2)	2.778(2)	Ru(1)−Ru(3)	2.726(2)
Ru(2)−Ru(3)	2.625(2)	Ru(2)−Ru(4)	2.839(2)
Ru(3)−Ru(4)	2.830(2)	Ru(1)−P(1)	2.356(4)
Ru(2)−P(1)	2.325(4)	Ru(1)−P(2)	2.406(5)
Ru(3)−P(2)	2.311(5)	Ru(1)−C(10)	2.03(1)
Ru(2)−C(10)	2.36(2)	Ru(2)−C(11)	2.29(1)
Ru(3)−C(10)	2.29(2)	Ru(3)−C(11)	2.39(1)
Ru(4)−C(12)	2.12(2)	C(10)−C(11)	1.32(2)
C(11)−C(12)	1.46(2)	C(18)−C(19)	1.19(2)
C(12)−C(13)	1.32(2)	C(19)−C(20)	1.38(2)
C(13)−C(18)	1.41(2)	C(20)−C(21)	1.23(3)
Ru(1)−Ru(2)−Ru(4)	121.53(7)	Ru(1)−Ru(3)−Ru(4)	123.82(7)
Ru(2)−Ru(4)−Ru(3)	55.15(5)	Ru(2)−Ru(1)−Ru(3)	56.96(5)
Ru(1)−P(1)−Ru(2)	72.79(13)	Ru(1)−P(2)−Ru(3)	70.23(14)
Ru(1)−C(10)−C(11)	145.8(12)	Ru(4)−C(12)−C(13)	134.4(12)
C(10)−C(11)−C(12)	172.9(15)	C(11)−C(12)−C(13)	129.0(15)
C(12)−C(13)−C(18)	119.7(16)	C(13)−C(18)−C(19)	177.9(19)
C(18)−C(19)−C(20)	176.0(19)	C(19)−C(20)−C(21)	175.1(22)

Both of the bond vectors from Ru(1) to the hinge atoms Ru(2) and Ru(3) (Ru(1)−Ru(2) 2.778(2) Å, Ru(1)−Ru(3) 2.725(2) Å) are supported by PPh_2 bridges. The unsupported edges formed by Ru(2)−Ru(4) and Ru(3)−Ru(4) are somewhat longer (2.839(2) and 2.830(2) Å, respectively). In a manner similar to that found in other electron-precise Ru_4 butterfly clusters, the closest Ru−Ru contact is found between the atoms of the hinge (Ru(2)−Ru(3) 2.625(2) Å).[10] In the solid-state structure, the C(4)−O(4) carbonyl ligand is found to be semibridging the Ru(2)−Ru(4) vector (Ru(2)−C(4) 1.94(2) Å; Ru(4)−C(4) 3.12(2) Å; Ru(2)−C(4)−O(4) 168(1)°). The most striking feature of **2** is the C_8 hydrocarbon chain which is attached to the metal framework via atoms C(10), C(11), and C(12). Evidently, this ligand originates from the head to tail coupling of two diyne units on the

(10) (a) Corrigan, J. F.; Doherty, S.; Taylor, N. J.; Carty, A. J. *Organometallics* **1993**, *12*, 993. (b) Housecroft, C. E.; Matthews, D. M.; Rheingold, A. L.; Song, X. *J. Chem. Soc., Dalton Trans.* **1992**, 2855. (c) Van Gastel, F.; Corrigan, J. F.; Doherty, S.; Taylor, N. J.; Carty, A. J. *Inorg. Chem.* **1992**, *31*, 4492.

cluster core. The bond lengths associated with the carbon chain suggest considerable delocalization over its entire length for both metal-bound and pendant portions. The Ru(1)−Ru(2)−Ru(3) fragment may be viewed as supporting the acetylide-like C(10)−C(11) atoms in the usual μ_3-η^1,η^2,η^2 fashion. The C(10)−C(11) distance in **2** (1.32(2) Å) is slightly longer than that found in $Ru_3(CO)_6(\mu\text{-}CO)_2(\mu\text{-}PPh_2)(\mu_3\text{-}\eta^1,\eta^2\text{-}C{\equiv}CBu^t)$ (1.242(5) Å)[11] and presumably reflects the greater scope for delocalization of charge in the case of **2**. The C(10)−C(11)−C(12) portion of the ligand in **2** is near linear (172.8(1)°) as a result of C(12) being bonded to the fourth ruthenium atom. It is also interesting to note the pattern of metal−metal bond lengths in the trinuclear acetylide complex where the shortest bond (2.708(5) Å) is that perpendicular to the acetylide vector, as in **2**. One may formally view the rest of the hydrocarbyl ligand in **2** as a vinyldiynyl unit, coordinated via C(12) to both C(11) and wing-tip atom Ru(4). The vinyl linkage is representative of sp^2 hybridization of C(12) and C(13) (1.33(2) Å) with the latter bearing a Bu^t and diynyl substituent (C(13)−C(18) 1.41(2) Å, C(18)−C(19) 1.19(3) Å, C(19)−C(20) 1.38(3) Å, C(20)−C(21) 1.23(3) Å, and C(21)−C(22) 1.46(4) Å).

In terms of electron counting, tetranuclear clusters with five M−M bonds, such as **2**, are predicted to have 62 valence electrons according to the EAN rule. This formula is satisfied for **2** if the $C_8(Bu^t)_2$ ligand serves as a six-electron donor. By contrast, the related electron-rich bis(phosphido)-bridged butterfly clusters $Ru_4(CO)_{13}(\mu\text{-}PR_2)_2$ all show expanded metal frameworks as a result of their 64-electron counts.[12]

In an attempt to establish the route by which **2** is formed, a sample of the dinuclear complex $Ru_2(CO)_6(\mu\text{-}PPh_2)(\mu\text{-}\eta^1,\eta^2\text{-}C{\equiv}C{-}C{\equiv}CBu^t)$ (**1a**) was thermolyzed in refluxing THF for 4 h. Cluster **2** (13%) was identified as one of the eight products formed. Thus, while the mechanism by which **2** is formed is not clear, it is likely that dimerization of **1a** in a manner similar to that previously observed for the related acetylide compound $Ru_2(CO)_6(\mu\text{-}PPh_2)(\mu\text{-}\eta^1,\eta^2\text{-}C{\equiv}CBu^t)$ is involved.[13]

The thermolysis of $Ru_3(CO)_{11}(Ph_2PC{\equiv}C{-}C{\equiv}CBu^t)$ also yielded small amounts of cluster **3**, $Ru_4(CO)_{10}(\mu\text{-}CO)(\mu_4\text{-}PPh)\{\mu_4\text{-}\eta^1,\eta^1,\eta^2,\eta^2\text{-}(Bu^tC{\equiv}C)C{\equiv}CPh\}$, the molecular structure of which is depicted in Figure 2. The

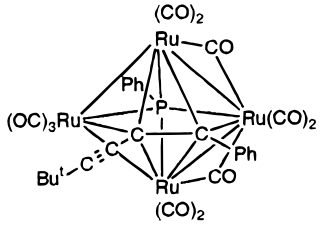

3

metal core of cluster **3** consists of four Ru atoms in a distorted square-planar arrangement. One face of the square is capped by a μ_4-phosphinidene ligand and the

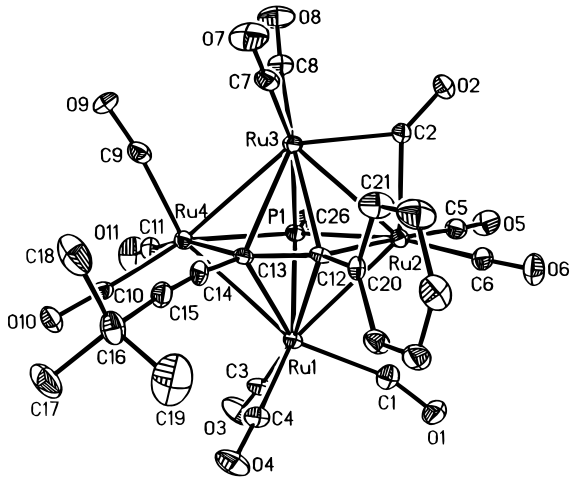

Figure 2. Molecular structure and numbering scheme for **3**. Only the *ipso*-carbon of the phosphido ligand is shown, and phenyl and Bu^t hydrogen atoms have been omitted for clarity.

other by a 1,1-dimethyl-4-phenylpenta-2,4-diyne ligand, which is coordinated via one C≡C moiety. Analogous species have been previously obtained in this laboratory from the reaction of diynes RC≡CC≡CR (R = Ph, Me, $SiMe_3$) with the *nido* butterfly cluster $Ru_4(CO)_{13}(\mu_3\text{-}PPh)$.[14] Structural parameters associated with **3** (Table 2) are similar to those observed in the MeC≡CC≡CMe species. Thus, the pattern of M−M distances in **3** is one short (Ru(2)−Ru(3) 2.731(1) Å) and three normal (2.825(1)−2.889(1) Å) bond lengths with the former supporting the bridging CO group. The situation is similar in the chalcogenide-containing clusters $Ru_4(CO)_{10}(\mu\text{-}CO)(\mu_4\text{-}PPh)(\mu_4\text{-}S)$ and $Ru_4(CO)_9(\mu\text{-}CO)(\mu_4\text{-}PPh)(\mu_4\text{-}Se)(PEt_3)$ with the μ-carbonyl ligand bridging a contracted M−M edge.[15] The C_4 chain in **3** is bound to the metal square via C(12)−C(13) with σ interactions to Ru(2) and Ru(4) (Ru(2)−C(12) 2.166(5) Å, Ru(4)−C(13) 2.132(6) Å) and longer η^2-interactions to Ru(1) and Ru(3) (Ru(1)−C(12) 2.346(6) Å, Ru(1)−C(13) 2.378(6) Å, Ru(3)−C(12) 2.376(5) Å, Ru(3)−C(13) 2.471(6) Å). The consequent rehybridization of these coordinated quaternary carbons results in a C(12)−C(13)−C(14) angle of 116.6(5)° (cf. 116.4(5)° in $Ru_4(CO)_{10}(\mu\text{-}CO)(\mu_4\text{-}PPh)\{\mu_4\text{-}\eta^1,\eta^1,\eta^2,\eta^2\text{-}(MeC{\equiv}C)C{\equiv}CMe\}$[14]). Partial delocalization along the butadiyne group is reflected in C−C distances (C(12)−C(13)1.423(7) Å, C(13)−C(14) 1.448-(7) Å, C(14)−C(15) 1.192(8) Å) which mirror those found in the MeC_4Me cluster.

Clearly, one step in the formation of **3** is the migration of a Ph group from a phosphido ligand to the diynyl ligand. Phenyl migration reactions are not uncommon in organic[16] and organometallic chemistry,[17] and there are several examples of phenyl ligand transfers from phosphine ligands.[18]

(11) Nucciarone, D.; MacLaughlin, S. A.; Taylor, N. J.; Carty, A. J. *Organometallics* **1988**, *7*, 106.
(12) Corrigan, J. F.; Sun, Y.; Carty, A. J. *New J. Chem.* **1994**, *18*, 77 and references therein.
(13) Chi, Y.; Carty, A. J.; Blenkiron, P.; Delgado, E.; Enright, G. D.; Wang, W.; Peng, S.-M.; Lee, G.-H. *Organometallics* **1996**, *15*, 5269.
(14) Corrigan, J. F.; Doherty, S.; Taylor, N. J.; Carty, A. J. *Organometallics* **1993**, *12*, 1365.
(15) Van Gastel, F.; Agocs, L.; Cherkas, A. A.; Corrigan, J. F.; Doherty, S.; Ramachandran, R.; Taylor, N. J.; Carty, A. J. *J. Cluster Sci.* **1991**, *2*, 131.
(16) Murray, A. W. *Organic Reaction Mechanisms*. Knipe, A. C., Watts, W. E., Eds. Wiley: New York, 1984; Chapter 15, p 431.
(17) (a) Blenkiron, P.; Enright, G. D.; Taylor, N. J.; Carty, A. J. *Organometallics* **1996**, *15*, 2855. (b) Bly, R. S.; Zhong, Z.; Kane, C.; Bly, R. K. *Organometallics* **1994**, *13*, 899 and references therein.
(18) Taylor, N. J.; Chieh, P. C.; Carty, A. J. *J. Chem. Soc., Chem. Commun.* **1975**, 448.

The remaining PPh fragment is trapped as a μ_4 phosphinidene ligand. In the ^{31}P NMR spectrum, this ligand gives rise to a characteristically low-field resonance (δ 251.5) typical of 62-electron $Ru_4(CO)_{10}(\mu$-CO)-(μ_4-X)(μ_4-Y) species.[19] Interestingly, the diyne ligand in cluster **3** is attached via the Ph−C≡C moiety, leaving the Bu^t−C≡C portion uncoordinated. This presumably reflects a combination of electronic and steric factors. In the ^{13}C NMR spectrum, the four diynyl carbons are observed as singlets (δ 145.6, 117.8, 110.9, 77.2) with the highest frequency signal probably representing the *C*−Ph atom. The carbonyl ligands exchange rapidly on the NMR time scale and are observed as a single peak (δ 200.75, d, J_{PC} 12.3 Hz), as was the case with the analogous $Ru_4(CO)_{10}(\mu$-CO)(μ_4-PPh){μ_4-η^1,η^1,η^2,η^2-(MeC≡C)C≡CMe} cluster.[14]

The cluster may also be viewed as a pentagonal bipyramid, the basal plane being defined by Ru(2), C(12), C(13), Ru(4), and P(1). In terms of electron counting, cluster **3** correlates well with the predictions of PSEPT theory[20] with a closo-type structure derived from seven vertices and eight skeletal pairs, in which the C_4 moiety donates six electrons to the cluster core as two alkylidyne (C2) ligands.

The thermolysis of $Ru_3(CO)_{11}(Ph_2PC{\equiv}C{-}C{\equiv}CBu^t)$ also generated small quantities of $Ru_4(CO)_{10}(\mu_4$-PPh)-(μ_4-η^1,η^1,η^3,η^3-PhC≡CC≡CBu^t) (**4**; 3%), which was characterized by the usual spectroscopic techniques, elemental microanalysis, and a single-crystal X-ray diffraction study (*vide infra*).

It has been demonstrated that clusters similar to **3** are converted to the bis-μ-(alkylidyne)dicarbide-like species $Ru_4(CO)_{10}(\mu_4$-PPh)(μ_4-η^1,η^1,η^3,η^3-RC≡CC≡CR) via thermally-induced CO loss in heptane or toluene solutions.[14] In a separate experiment, we found that thermolysis of cluster **3** also yields cluster **4**, with quantitative conversion being achieved after just 20 min (cf. 8 and 4 h, respectively, for the PhC≡CC≡CPh and $Me_3SiC{\equiv}CC{\equiv}CSiMe_3$ analogues[14]).

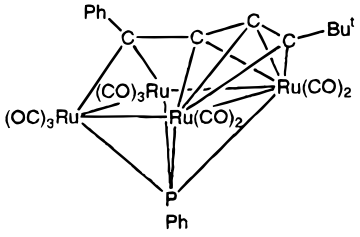

4

In keeping with the established trends, **4** exhibits a downfield resonance at 446 ppm in the ^{31}P NMR spectrum, which is in the region characteristic of a μ_4-phosphinidene ligand face capping an electron-precise, square Ru_4 cluster.[21] Despite the loss of a CO ligand, there is an overall increase of two electrons in the CVE of **4** (64 electrons) compared to **3** (62 electrons) as the diyne ligand transforms from a four-electron-donating μ_4-η^1,η^1,η^2,η^2- bonding mode to an eight-electron-donor μ_4-η^1,η^1,η^3,η^3- ligand by incorporating the formerly pendant −C≡CBu^t moiety into the organometallic framework.

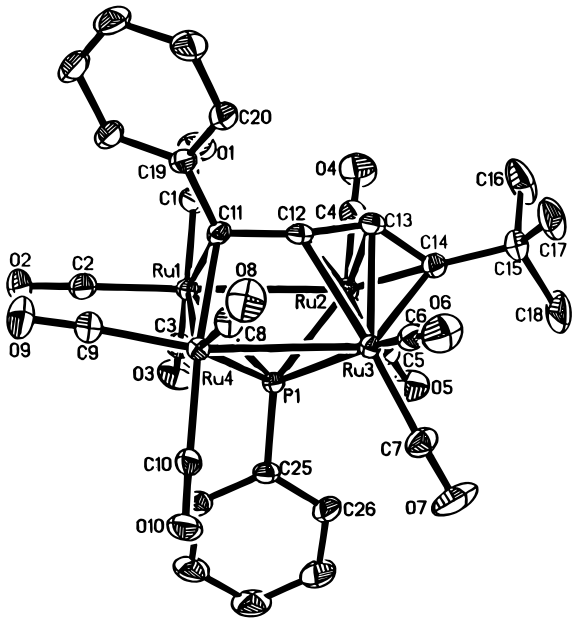

Figure 3. Molecular structure and numbering scheme for **4**. Hydrogen atoms have been omitted for clarity.

Table 3. Selected Bond Distances (Å) and Angles (deg) for Cluster 3

Ru(1)−Ru(2)	2.825(1)	Ru(1)−Ru(4)	2.839(1)
Ru(3)−Ru(4)	2.889(1)	Ru(2)−Ru(3)	2.731(1)
Ru(1)−P(1)	2.417(2)	Ru(2)−P(1)	2.392(2)
Ru(3)−P(1)	2.477(2)	Ru(4)−P(1)	2.362(2)
Ru(1)−C(12)	2.346(6)	Ru(1)−C(13)	2.378(6)
Ru(3)−C(12)	2.376(5)	Ru(3)−C(13)	2.471(6)
Ru(2)−C(12)	2.166(5)	Ru(4)−C(13)	2.132(6)
C(20)−C(12)	1.509(8)	C(12)−C(13)	1.423(7)
C(13)−C(14)	1.448(7)	C(14)−C(15)	1.192(8)
Ru(1)−Ru(2)−Ru(3)	85.4(1)	Ru(2)−Ru(3)−Ru(4)	94.5(1)
Ru(3)−Ru(4)−Ru(1)	82.3(1)	Ru(4)−Ru(1)−Ru(2)	93.6(1)
C(12)−C(13)−C(14)	116.6(5)	C(13)−C(14)−C(15)	174.3(7)

The molecular structure of $Ru_4(CO)_{10}(\mu_4$-PPh)(μ_4-η^1,η^1,η^3,η^3-PhC≡C−C≡CBu^t) (**4**) is depicted in Figure 3 with key bond distances and angles listed in Table 4. As has been indicated above, the metal core of cluster **4** is composed of a distorted square of Ru atoms, capped on one face by a μ_4-phosphinidene ligand and on the other by the diyne ligand, which is now attached to the metal framework through all four carbon atoms. Metal−metal bond lengths span a range with the shortest being that supported by three of the four diyne carbon atoms (Ru(2)−Ru(3) 2.680(1) Å). Of the others, one is of normal length (Ru(1)−Ru(4) 2.839(1) Å) while two are somewhat elongated (Ru(1)−Ru(2) 2.950(1) Å, Ru(3)−Ru(4) 2.978(1) Å). The structural characteristics of the hydrocarbyl group in **4** are similar to those reported for the Bu^{t}C≡C−C≡CBu^t [22] and SiMe$_3$C≡C−C≡CSiMe$_3$[14]

(19) (a) Mathur, P.; Charkrabarty, D.; Hossain, M. M. *J. Organomet. Chem.* **1991**, *418*, 415. (b) Mathur, P.; Mavunkal, I. J.; Rugmini, V.; Mahon, M. F. *Inorg. Chem.* **1990**, *29*, 4838. (c) Adams, R. D.; Babin, J. E.; Tasi, M. *Inorg. Chem.* **1990**, *29*, 4658. (d) Adams, R. D.; Babin, J. E.; Estrada, J.; Wang, J. G.; Hall, M. B.; Low, M. M. *Polyhedron* **1989**, *8*, 1885. (e) Braunstein, P. *New J. Chem.* **1986**, *10*, 365.

(20) (a) Wade, K. *Adv. Inorg. Chem. Radiochem.* **1976**, *18*, 1. (b) Wade, K. In *Transition Metal Clusters*; Johnson, B. F. G., Ed.; John Wiley and Sons Publishers: New York, 1981; p 193. (c) Mingos, D. M. P. *Acc. Chem. Res.* **1984**, *17*, 311. (d) Mingos, D. M. P.; Wales, D. J. *Introduction to Cluster Chemistry*; Prentice Hall Publishers: Eaglewood Cliffs, NJ, 1990.

(21) Carty, A. J.; MacLaughlin, S. A.; Nucciarone, D. *In Phosphorus-31 NMR Spectroscopy in Stereochemical Analysis: Organic Compounds and Metal Complexes*; Verkade, J. G., Quinn, L. D., Eds.; VCH: New York, 1987; Chapter 16, pp 559−619.

Table 4. Selected Bond Distances (Å) and Angles (deg) for Cluster 4

Ru(1)−Ru(2)	2.950(1)	Ru(1)−Ru(4)	2.839(1)
Ru(3)−Ru(4)	2.978(1)	Ru(2)−Ru(3)	2.680(1)
Ru(1)−P(1)	2.181(3)	Ru(2)−P(1)	2.354(1)
Ru(3)−P(1)	2.379(1)	Ru(4)−P(1)	2.399(1)
Ru(1)−C(11)	2.181(3)	Ru(4)−C(11)	2.178(2)
Ru(2)−C(12)	2.339(3)	Ru(2)−C(13)	2.224(3)
Ru(2)−C(14)	2.118(3)	Ru(3)−C(12)	2.339(3)
Ru(3)−C(13)	2.229(2)	Ru(3)−C(14)	2.123(3)
C(19)−C(11)	1.500(4)	C(11)−C(12)	1.415(4)
C(12)−C(13)	1.298(4)	C(13)−C(14)	1.404(4)
Ru(1)−Ru(2)−Ru(3)	92.3(1)	Ru(2)−Ru(3)−Ru(4)	90.7(1)
Ru(3)−Ru(4)−Ru(1)	88.7(1)	Ru(4)−Ru(1)−Ru(2)	83.3(1)
C(19)−C(11)−C(12)	116.2(2)	C(11)−C(12)−C(13)	171.1(3)
C(12)−C(13)−C(14)	137.0(3)	C(13)−C(14)−C(15)	130.8(3)

analogues. Thus, the formerly acetylenic C(11)−C(12) and C(13)−C(14) bonds are elongated to 1.415(4) and 1.404(4) Å, respectively, with the central C(12)−C(13) (1.298(4) Å) linkage now exhibiting significant multiple-bond character. Evidently substantial rehybridization of the diynyl carbons has occurred as a result of both acetylene units binding to the cluster face (C(19)−C(11)−C(12) 116.2(2)°, C(11)−C(12)−C(13) 171.1(3)°, C(12)−C(13)−C(14) 137.0(3)°).

Orange crystals of $Ru_5(CO)_{11}(\mu\text{-}CO)(\mu\text{-}PPh_2)_2(\mu_3\text{-}\eta^1,\eta^1,\eta^1\text{-}C{\equiv}C{-}C{\equiv}CBu^t)(\mu_4\text{-}C)(\mu_2\text{-}\eta^1,\eta^1\text{-}C{-}C{\equiv}CBu^t)$ (**5**) were obtained as the major component of an orange band, which also contained cluster **3**. The ^{31}P NMR spectrum of **5**

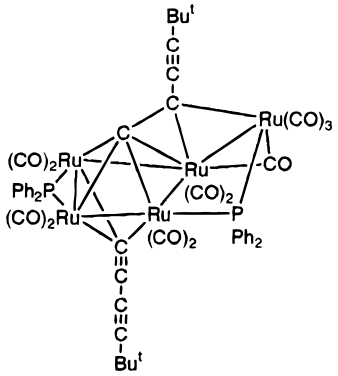

5

exhibits two singlet resonances at 54.7 and 209.6 ppm, characteristic of phosphido groups bridging open and closed Ru−Ru edges, respectively. The absence of P−P coupling in the spectrum indicated that these ligands were significantly removed from each other. Peaks corresponding to two Bu^t groups in the ^1H spectrum corroborate the presence of four Ph groups (by integration), which is consistent with the ^{31}P data. The ^{13}C NMR spectrum contained at least seven resonances that could be assigned to quaternary carbons, as well as two sets of resonances at higher field consistent with two Bu^t groups.

A single-crystal X-ray analysis was carried out, and a molecule of **5** is dipicted in Figure 4, while selected bond parameters are collected in Table 5. The metal framework consists of a distorted spiked square with Ru−Ru bonds within the expected range (2.736(1)−2.877(1) Å). The spiked atom Ru(5) is bound to three bridging groups, namely, the μ-CO ligand via C(3), a PPh_2 group via P(1), and C(14) of the C_4 chain. The latter is bonded to the metal skeleton through the

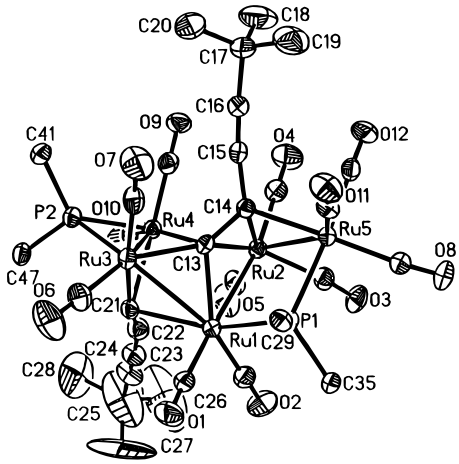

Figure 4. Molecular structure and numbering scheme for **5**. Only the *ipso*-carbons of the phenyl groups are shown, and hydrogen atoms have been omitted for clarity.

Table 5. Selected Bond Distances (Å) and Angles (deg) for Cluster 5

Ru(1)−Ru(2)	2.877(1)	Ru(1)−Ru(3)	2.865(1)
Ru(2)−Ru(4)	2.834(1)	Ru(2)−Ru(5)	2.823(1)
Ru(3)−Ru(4)	2.736(1)	Ru(1)−P(1)	2.322(1)
Ru(5)−P(1)	2.408(1)	Ru(3)−P(2)	2.292(1)
Ru(4)−P(2)	2.322(1)	Ru(1)−C(13)	2.126(3)
Ru(2)−C(13)	2.164(4)	Ru(3)−C(13)	2.131(4)
Ru(4)−C(13)	2.302(4)	Ru(2)−C(14)	2.187(4)
Ru(5)−C(14)	2.159(4)	Ru(1)−C(21)	2.291(4)
Ru(3)−C(21)	2.023(5)	Ru(4)−C(21)	2.383(3)
C(13)−C(14)	1.407(6)	C(14)−C(15)	1.433(5)
C(15)−C(16)	1.191(6)	C(21)−C(22)	1.233(7)
C(22)−C(23)	1.391(8)	C(23)−C(24)	1.199(9)
Ru(1)−Ru(2)−Ru(4)	74.4(1)	Ru(2)−Ru(4)−Ru(3)	96.1(1)
Ru(4)−Ru(3)−Ru(1)	76.1(1)	Ru(3)−Ru(1)−Ru(2)	92.4(1)
Ru(4)−Ru(2)−Ru(5)	126.3(1)	Ru(1)−P(1)−Ru(5)	105.1(1)
Ru(3)−P(2)−Ru(4)	72.7(1)	C(13)−C(14)−C(15)	124.7(4)
C(14)−C(15)−C(16)	170.6(5)	C(21)−C(22)−C(23)	164.5(5)
C(22)−C(23)−C(24)	176.2(5)		

C(13)−C(14) unit (1.407(6) Å), which has become substantially elongated relative to the pendant outer alkyne group C(15)−C(16) (1.191(6) Å). The attachment of C(13) to four metal atoms (Ru(1)−Ru(4)) as well as to C(14) lends carbidic character to the former. Indeed, this is supported by the ^{13}C NMR data which shows a resonance at 294.5 ppm (d, J_{PC} 16 Hz), a region usually associated with transition-metal carbide ligands.[23] The bridging alkylidyne atom C(14) is linked to the alkynyl carbon C(15) via a short single bond (C(14)−C(15) 1.433(5) Å) and to the carbidic carbon C(13) and, thus, allows the C(13)−C(14) moiety to be best considered as an alkylidyne carbide ligand.

The structure reveals the presence of a second C_4 fragment, attached to the triangular Ru(1)−Ru(3)−Ru(4) face via C(21), and provides a rare example of a μ_3-η^1 diynyl group. The latter is attached to the metal core through one short (Ru(3)−C(21) 2.023(5) Å) and two long (Ru(1)−C(21) 2.291(4) Å, Ru(4)−C(21) 2.383(3) Å) M−C interactions. In fact, these values mirror those reported for the complex $Ru_3(CO)_6(\mu\text{-}CO)_2(\mu\text{-}PPh_2)(\mu_3\text{-}\eta^1,\eta^2\text{-}C{\equiv}C\text{-}Bu^t)$, in which the Ru−$C_\sigma$ bond is considerably shorter

(22) Bobbie, B. J.; Taylor, N. J.; Carty, A. J. *J. Chem. Soc., Chem. Commun.* **1991**, 1511.

(23) (a) Mason, J. *J. Am. Chem. Soc.* **1991**, *113*, 24. (b) Bradley, J. S. *Adv. Organomet. Chem.* **1983**, *22*, 1. (c) Johnson, B. F. G.; Lewis, J.; Nelson, W. J. H.; Nicholls, J. N.; Vargas, M. D. *J. Organomet. Chem.* **1983**, *249*, 255.

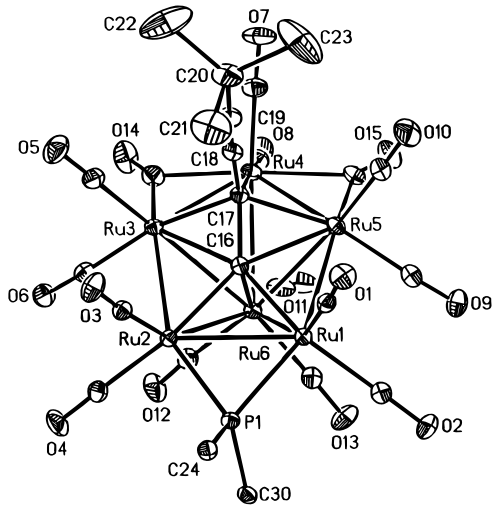

Figure 5. Molecular structure and numbering scheme for **6a**. Only the *ipso*-carbons of the phenyl groups are shown, and hydrogen atoms have been omitted for clarity.

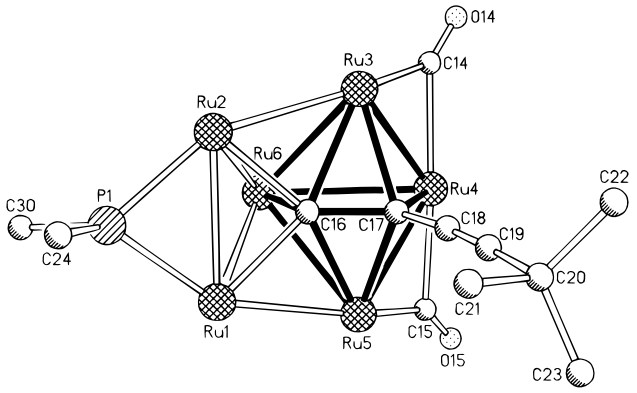

Figure 6. Molecular structure of **6a** highlighting the Ru_4C_2 octahedral core. Only the *ipso*-carbons of the phenyl groups are shown, and the carbonyl ligands and hydrogen atoms have been omitted for clarity.

than the Ru−C_π interactions, and reflects the relative strength of the Ru(3)−C(21) bond.

In the present case, the C(21)−C(22)−C(23) bond angle (164.5(5)°) is significantly less than 180°, perhaps suggesting weak interactions of C(22) with Ru(1) or Ru(2). However, the Ru(1)···C(22) and Ru(4)···(C22) contacts are longer than 3.0 Å, which would seem to rule out even weak bonding. The C(21)−C(22) separation (1.233(7) Å) is only slightly longer than that observed in free acetylene (1.2033(2) Å) and is close to the range 1.190−1.214 Å in which two-thirds of the η^1-alkynyl C≡C bond lengths surveyed have been found to fall.[24]

With five metal centers and the same number of M−M bonds, the EAN rule predicts an electron count of 80 for cluster **5**. Assuming a contribution of 1e for the η^1-butadiynyl ligand and 5e for the alkylidyne carbide group, **5** is in fact formally electron deficient (76e). Such a shortfall may account for the relatively short Ru(3)−Ru(4) bond (2.736(1) Å) and the observed distortion of the μ_3-η^1 diynyl ligand.

The sixth component of the reaction mixture to be fully characterized was the hexanuclear species $Ru_6(CO)_{13}(\mu\text{-CO})_2(\mu\text{-PPh}_2)(\mu_5\text{-C})(\mu_3\text{-}\eta^1,\eta^1,\eta^1\text{-C}{-}\text{C}{\equiv}\text{CR})$ **6a**.[9]

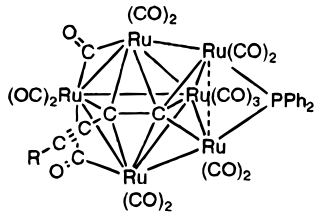

R = Bu^t (**6a**), Ph (**6b**)

The molecular structure of **6a** is shown in Figure 5. The six metal atoms and C(16) form a pentagonal bipyramid, although a closer examination of the structure indicates that the cluster is better described as a bicapped Ru_4C_2 octahedron (*vide infra*). This point of view is highlighted in Figure 6. The carbide-like carbon C(16) makesbonding contacts with five of the six Ru atoms of the cluster framework (Ru(1)−C(16) 2.108(4) Å, Ru(2)−C(16) 2.119(4) Å, Ru(3)−C(16) 2.271(4) Å, Ru(5)−C(16) 2.265(3) Å, Ru(6)−C(16) 2.103(4) Å) and with C(17) (C(16)−C(17) 1.458(7) Å). In turn, C(17) is attached to Ru(3), Ru(4), and Ru(5) (2.186(4), 2.194(3), 2.182(4) Å, respectively) as well as the pendant alkynyl moiety C(18)−C(19) (C(17)−C(18) 1.435(6) Å, C(18)−C(19) 1.197(6) Å), which leads us to describe the ligand as an alkylidyne carbide. The geometry of **6a** has been described in some detail in our earlier account.[9] A detailed examination of the electronic structure of this unusual cluster is presented below.

A related Ru_6 cluster $Ru_6(CO)_{12}(\mu\text{-CO})(\mu\text{-PPh}_2)_2(\mu_6\text{-}C_2\text{CH}{=}\text{CHBu}^t)(\mu_3\text{-}C_2\text{Bu}^t)$ bearing a $C_2CH{=}CHBu^t$ alkylidene carbide ligand, which is coordinated in a fashion similar to that described for the $C_2C{\equiv}CBu^t$ alkylidyne carbide ligand in **6**, has recently been reported by Bruce and co-workers.[25]

(b) Thermolysis of $Ru_3(CO)_{11}(Ph_2PC{\equiv}CC{\equiv}CR)$ (R = Ph, $SiMe_3$). The thermolysis of $Ru_3(CO)_{11}(Ph_2PC{\equiv}CC{\equiv}CPh)$[8] under similar conditions to those described for the Bu^t analogue yielded **1b**[8] and **6b** as the only isolable products. Cluster **6b** was readily identified by comparison of the spectral data with that of **6a** and will not be discussed further.

In the case of the $SiMe_3$-substituted complex $Ru_3(CO)_{11}(Ph_2PC{\equiv}CC{\equiv}CSiMe_3)$,[8] thermolysis and chromatographic workup failed to give any $SiMe_3$-substituted analogues of clusters **2**−**6**. Instead, the complexes $Ru_2(CO)_6(\mu\text{-PPh}_2)(\mu\text{-}\eta^1,\eta^2\text{-C}{\equiv}\text{C}{-}\text{C}{\equiv}\text{CSiMe}_3)$ (**1c**)[8] and $\{Ru_2(CO)_6(\mu\text{-PPh}_2)\}_2(\mu\text{-}\eta^1,\eta^2{:}\mu\text{-}\eta^1,\eta^2\text{-C}{\equiv}\text{C}{-}\text{C}{\equiv}\text{C}{-})$ (**7**) were obtained. Under our reaction conditions, the absence

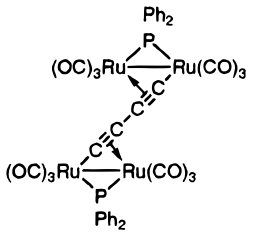

7

(24) Manna, J.; John, K. D.; Hopkins, M. D. *Adv. Organomet. Chem.* **1989**, *38*, 79.

(25) Bruce, M. I.; Humphrey, P. A.; Skelton, B. W.; White, A. H. *J. Chem. Soc., Dalton Trans.* **1997**, 1485.

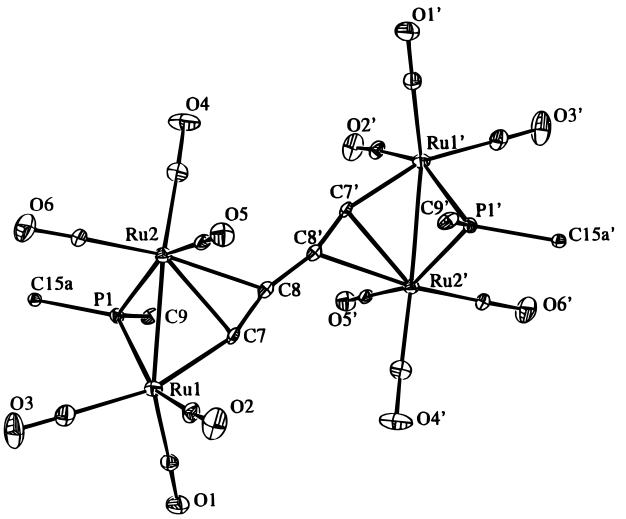

Figure 7. Molecular structure and numbering scheme for **7**. Only the *ipso*-carbons of the phenyl groups are shown.

of analogues may be due to facile cleavage of the C−$SiMe_3$ bond. Compound **7** was characterized by the usual spectroscopic techniques and a single-crystal X-ray study (*vide infra*). Bruce and co-workers have reported the analogous Fe complex $\{Fe_2(CO)_6(\mu\text{-}PPh_2\}_2(\mu\text{-}C_4)$, which was obtained in 12% yield from reaction of the bis(phosphino)diyne complex $(CO)_4Fe{-}Ph_2PC{\equiv}C{-}C{\equiv}CPPh_2{-}Fe(CO)_4$ with $Fe_2(CO)_9$.[7c]

The ν(CO) region of the IR spectrum indicated the presence of only terminal CO ligands. The ^{1}H and ^{13}C NMR spectra contained resonances arising from the phenyl rings of the μ-PPh_2 ligands. The latter also contained two diyne signals due to C_α (δ 103.3, d, J_{PC} 27 Hz) and C_β (δ 129.0, d, J_{PC} 12 Hz), which were assigned on the basis of the magnitude of the J_{PC} coupling constants, and three doublet resonances (J_{PC} = 12, 72, 6 Hz) from the CO ligands. A ^{31}P signal at δ 121.8 in **7** is consistent with a closed μ-PPh_2 group and, indeed, is virtually identical to that observed for **1c** (δ 122.0) and other complexes of this type.

The structural investigation revealed the presence of two $Ru_2(CO)_6(\mu\text{-}PPh_2)$ fragments, each attached in a μ-η^1,η^2 fashion to a *trans* bent butadiynyl ligand. The molecule is shown in Figure 7 and may be viewed as a dimer of $[Ru_2(CO)_6(\mu\text{-}PPh_2)(\mu\text{-}\eta^1,\eta^2\text{-}C{\equiv}C)]$, with rotational symmetry about the central C(8)−C(8′) single bond. The geometries of the phosphido-bridged $Ru_2(CO)_6$ cores (Table 7) are similar to those found in other examples of this class of compound, such as $Ru_2(CO)_6(\mu\text{-}\eta^1,\eta^2\text{-}C{\equiv}CBu^t)(\mu\text{-}PPh_2)$ (**8**)[5c] (cf Ru(1)−Ru(2) 2.7608(10) Å (**7**), 2.7523(3) Å (**8**); Ru(1)−P 2.3549(23) Å (**7**), 2.3399(8) Å (**8**); Ru(1)−C(7) 2.049(8) Å (**7**), 2.044(3) Å (**8**); Ru(2)−C(7) 2.296(8) Å (**7**), 2.285(3) Å (**8**); Ru(2)−C(8) 2.446(8) Å (**7**), 2.417(3) Å (**8**); Ru(1)−P−Ru(2) 71.66(6)° (**7**), 72.03(1)° (**8**); P−Ru(1)−C(7) 77.09(22)° (**7**), 75.8(1)° (**8**); Ru(1)−Ru(2)−C(7) 46.68(19)° (**7**), 46.8(1)° (**8**); Ru(1)−C(7)−C(8) 160.0(7)° (**7**), 158.9(1)° (**8**)).

The primary interest in this structure comes from the interaction of the binuclear metal fragments through the four-carbon bridge. While the central C(8)−C(8′) bond (1.41(1) Å) is somewhat longer than that observed in the analogous iron compound (1.371(8) Å), the planar nature of the Ru_4C_4 core (maximum deviation from plane 0.10(1) Å) provides evidence for some degree of

Table 6. Selected Bond Distances (Å) and Angles (deg) for Cluster 6a

Ru(1)−Ru(2)	2.782(1)	Ru(2)−Ru(3)	2.756(1)
Ru(3)−Ru(4)	2.656(1)	Ru(4)−Ru(5)	2.671(1)
Ru(5)−Ru(1)	2.775(1)	Ru(1)−Ru(6)	2.916(1)
Ru(2)−Ru(6)	2.876(1)	Ru(3)−Ru(6)	2.861(1)
Ru(4)−Ru(6)	3.032(1)	Ru(5)−Ru(6)	2.814(1)
Ru(1)−P(1)	2.289(1)	Ru(2)−P(1)	2.276(1)
Ru(1)−C(16)	2.108(4)	Ru(2)−C(16)	2.119(4)
Ru(3)−C(16)	2.271(4)	Ru(5)−C(16)	2.265(3)
Ru(6)−C(16)	2.103(4)	Ru(3)−C(17)	2.186(4)
Ru(4)−C(17)	2.194(3)	Ru(5)−C(17)	2.182(4)
C(16)−C(17)	1.458(7)	C(17)−C(18)	1.435(6)
C(18)−C(19)	1.197(6)		
Ru(1)−Ru(2)−Ru(3)	101.8(1)	Ru(2)−Ru(3)−Ru(4)	120.0(1)
Ru(3)−Ru(4)−Ru(5)	93.7(1)	Ru(4)−Ru(5)−Ru(1)	120.0(1)
Ru(5)−Ru(1)−Ru(2)	101.2(1)	Ru(1)−P(1)−Ru(2)	75.1(1)
Ru(2)−C(16)−Ru(6)	85.9(1)	Ru(1)−C(16)−Ru(6)	87.7(2)
Ru(5)−C(16)−Ru(6)	80.1(1)	Ru(3)−C(16)−Ru(6)	81.6(1)
C(16)−C(17)−C(18)	121.8(3)	C(17)−C(18)−C(19)	175.1(5)

Table 7. Selected Bond Distances (Å) and Angles (deg) for Cluster 7

Ru(1)−Ru(2)	2.7608(10)	Ru(1)−P(1)	2.355(2)
Ru(1)−C(7)	2.049(8)	Ru(2)−P(1)	2.361(2)
Ru(2)−C(7)	2.296(8)	Ru(2)−C(8)	2.446(8)
C(8)−C(8a)	1.41(1)	Ru(1)−C(1)	1.907(9)
Ru(1)−C(2)	1.931(9)	Ru(1)−C(3)	1.965(9)
Ru(2)−C(4)	1.920(9)	Ru(2)−C(5)	1.944(8)
Ru(2)−C(6)	1.870(8)		
Ru(2)−Ru(1)−P(1)	54.28(6)	Ru(2)−Ru(1)−C(1)	147.2(2)
Ru(2)−Ru(1)−C(2)	98.7(3)	Ru(2)−Ru(1)−C(7)	54.6(2)
Ru(1)−C(7)−C(8)	160.0(7)	Ru(2)−C(7)−C(8)	81.9(6)
Ru(1)−Ru(2)−C(7)	46.7(2)	Ru(1)−Ru(2)−C(8)	76.3(2)
C(7)−C(8)−C(8a)	163.1(9)	Ru(2)−Ru(1)−C(1)	147.2(2)
Ru(2)−Ru(1)−C(2)	98.7(3)	Ru(2)−Ru(1)−C(3)	108.7(3)
Ru(1)−Ru(2)−C(4)	157.1(2)	Ru(1)−Ru(2)−C(5)	99.0(2)
Ru(1)−Ru(2)−C(6)	96.9(3)		

delocalization of electron density over the eight atoms. While there are electronic interactions between multi metallic cores linked by η^2,η^2-butadiyne ligands,[26] recent studies with linear, bimetallic systems have shown that η^1,η^1-butadiynediyl ligands are the most efficient electronic bridges that have been constructed between organometallic fragments to date.[27] Compound **7** and the analogous iron compound are curious examples of systems containing both of these bonding features and as such represent stepping stones between the rodlike butadiynediyl complexes and the ever-increasing number of cluster compounds containing 1,3-diyne ligands, in which the metal−carbon bonding occurs primarily through π-interactions.

(ii) Electron-Counting and EHMO Studies of $Ru_6(CO)_{13}(\mu\text{-}CO)_2(\mu\text{-}PH_2)(\mu_5\text{-}C)(\mu_3\text{-}\eta^1,\eta^1,\eta^1\text{-}C{-}C{\equiv}CH)$. The cluster **6a** has several unusual structural features: it is the first ruthenium cluster with a metal framework geometry which approximates a pentagonal pyramid; a single carbon atom C(16) is bound to five metal atoms in an environment which bears some resemblance to μ_5-carbides in pentanuclear systems such as $Ru_5(CO)_{15}(\mu_5\text{-}C)$; C(16) is also attached via a relatively long C−C bond to C(17) (C(16)−C(17) 1.458(7) Å), which itself is bonded in a μ_3-alkylidyne fashion on an open Ru_3 face. These unprecedented structural features pose interesting questions for electron count-

(26) McAdam, C. J.; Duffy, N. W.; Robinson, B. H.; Simpson, J. *Organometallics* **1996**, *15*, 3935 and references therein.
(27) Weyland, T.; Lapinte, C.; Frapper, G.; Calhorda, M. J.; Halet, J.-F.; Toupet, L. *Organometallics* **1997**, *16*, 2024.

ing and bonding in **6a**, prompting a detailed EHMO analysis.

(a) Electron-Counting Considerations. As pointed out above, the Ru_6 core of cluster **6a** can be viewed as a distorted pentagonal pyramid. From a PSEPT[20] viewpoint, this polyhedron is a *nido*-type cluster for which an 8 skeletal electron pair (SEP) count is expected, i.e., 88 cluster valence electrons (CVE). The application of the EAN rule to the Ru atoms, assuming 10 localized 2-electron Ru−Ru bonds, also leads to a predicted 88-CVE count. The actual CVE count associated with the Ru_6 core of cluster **6a** depends on the number of electrons donated to the metal framework by the C_4Bu^t ligand. Considering a formal bond order of three for the C(18)−C(19) bond and of one for C(17)−C(18), there are five nonbonding or π-bonding electrons localized on the C(16) and C(17) atoms. If all these electrons are donated to the Ru_6 core (i.e., there is no lone pair on C(16)), the electron count is 86 CVEs. Therefore, to reach the PSEPT or EAN expected 88-CVE count, it is necessary to include the C(16)−C(17) σ-bonding pair. However, the C(16)−C(17) separation (1.458 Å), while somewhat elongated, is indicative of a significant bonding interaction between C(16) and C(17). It follows that on the basis of a simple electron-counting model, **6a** is not adequately described as a true pentagonal pyramid.

Another way to analyze the structure of compound **6a** is to consider C(16) and C(17) together with the metal atoms as vertices of a larger cluster cage. Conventional PSEPT electron-counting procedures require the inclusion of *all* the exo-skeleton electrons in the CVE count.[20] Therefore, in this model, all the electrons associated with C(16) and C(17), including the C(17)−C(18) σ-bonding pair, must be included in the CVE count. From this perspective, the CVE count associated with the skeleton of **6a** is 90.

This Ru_6C_2 polyhedron can be described in terms of the condensation of an irregular octahedron of Ru(3), Ru(4), Ru(5), Ru(6), C(16), and C(17) with a bicapped tetrahedron consisting of Ru(1), Ru(2), Ru(3), Ru(5), Ru(6), and C(16). These two fused deltahedra share the Ru(3), Ru(5), Ru(6), C(16) rhombus. For the octahedron, the PSEP theory[20] predicts a count of 7 SEPs, corresponding to 66 CVEs for a mixed Ru_4C_2 cage. For the bicapped tetrahedron, the expected count is 6 SEPs, i.e., 74 CVEs for a Ru_5C cluster. From the condensation principle,[20c,d] the CVE count of the resulting Ru_6C_2 is expected to be the sum of the CVE counts of the isolated Ru_4C_2 and Ru_5C clusters less the number of electrons characterizing the shared Ru_3C rhombus. The usual CVE count for a rhomboidal butterfly Ru_3C framework is 52 CVE, corresponding to an electron-precise system. Therefore, the overall CVE count predicted for the Ru_6C_2 cluster is 88 (66 + 74 − 52). The Ru_6C_2 core of cluster **6a**, which was found to have 90 CVEs, would appear to be electron rich with respect to the predictions of the PSEPT for condensed polyhedra.

A somewhat related description of the Ru_6C_2 polyhedron is to view it as an Ru(3)Ru(4)Ru(5)Ru(6)C(16)C(17) octahedron bicapped by the Ru(1)Ru(2) fragment. Mingos' capping principle[20c] indicates that adding one ML_n capping unit to a cluster should add 12 electrons to the CVE count of the octahedron (66). Depending on whether the Ru(1)−Ru(2) bond is considered as a two-electron localized system or not, the dinuclear capping unit should add 12 × 2 − 2 = 22 or 12 × 2 = 24 electrons. Thus, for this model, the predicted CVE count associated with the Ru_6C_2 cluster cage is either 88 (6 SEPs) or 90 (7 SEPs). The latter corresponds to the actual CVE of cluster **6a**.

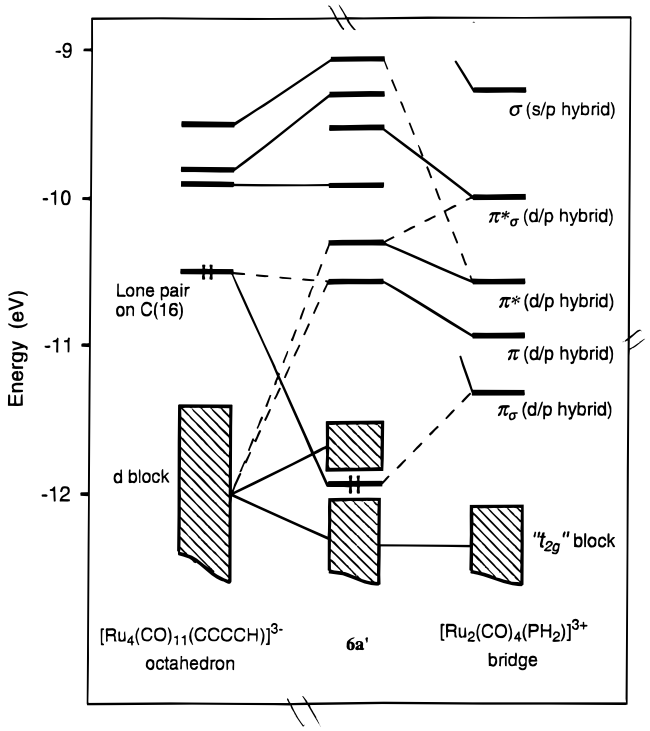

Figure 8. EHMO diagram of cluster **6a′** as resulting from the interaction of the $[Ru_4(CO)_9(\mu\text{-}CO)_2(\mu_5\text{-}C)(\mu_3\text{-}\eta^1,\eta^1,\eta^1\text{-}C{-}C{\equiv}CH)]^{3-}$ octahedron with the $[Ru_2(CO)_4(\mu\text{-}PH_2)]^{3+}$ bridge.

Table 8. Selected Overlap Populations Calculated for 6a′

Ru(1)−Ru(2)	0.100	Ru(6)−Ru(3)	0.151	Ru(4)−C(17)	0.353
Ru(2)−Ru(3)	0.152	Ru(6)−Ru(4)	0.100	Ru(5)−C(16)	0.168
Ru(3)−Ru(4)	0.147	Ru(6)−Ru(5)	0.168	Ru(5)−C(17)	0.246
Ru(4)−Ru(5)	0.130	Ru(1)−C(16)	0.419	Ru(6)−C(16)	0.423
Ru(5)−Ru(1)	0.143	Ru(2)−C(16)	0.404	C(16)−C(17)	0.920
Ru(6)−Ru(1)	0.084	Ru(3)−C(16)	0.165	C(17)−C(18)	0.964
Ru(6)−Ru(2)	0.111	Ru(3)−C(17)	0.249	C(18)−C(19)	1.885

(b) EHMO Calculations. To provide a better insight into the electronic structure of cluster **6a**, we have carried out EHMO calculations on the simplified model $Ru_6(CO)_{13}(\mu\text{-}CO)_2(\mu\text{-}PH_2)(\mu_5\text{-}C)(\mu_3\text{-}\ \eta^1,\eta^1,\ \eta^1\text{-}C{-}C{\equiv}CH)$ (**6a′**) with the geometry taken directly from the X-ray molecular structure of **6a** (*vide infra*). The MO diagram of **6a′** is shown in the middle of Figure 8. It exhibits a significant HOMO/LUMO gap of 0.90 eV for the actual 90-electron count of **6a** in agreement with its stability. This large gap is unique to the frontier orbital region, suggesting that the Ru_6C_2 polyhedron cannot accommodate electron counts which are different from its 90 CVE number. Some interatomic overlap populations are listed in Table 8. One can see that the strengths of the bonds are not necessarily reflected by the corresponding internuclear separations. For example, the particularly long Ru(6)−Ru(4) bond (3.032(1) Å) is calculated to be stronger than the shorter Ru(6)−Ru(1) bond (2.916(1) Å). Similarly, the unbridged Ru(1)−Ru(5) bond is much stronger than the almost equal but bridged Ru(1)−Ru(2) bond. Nevertheless, it is clear that

there is significant bonding along all of the Ru−Ru, Ru−C, and C−C vectors in the Ru_6C_2 cluster cage.

To analyze the pentagonal-pyramidal description of cluster **6a**, we first considered the electronic structure of the model **6a′** as formally resulting from the interaction of the $Ru_6(CO)_{15}(PH_2)$ fragment with the CCCCH ligand. Interestingly, the $Ru_6(CO)_{15}(PH_2)$ moiety does not present any significant HOMO/LUMO gap that would favor any one particular electron count. For example, the gaps corresponding to the 86- and 88-CVE counts are only 0.17 and 0.15 eV, respectively. The reason lies in the highly distorted character of the pentagonal pyramid, in particular the nonplanarity of the pentagonal base and the distribution of its bond angles (94−120°) which are far from the ideal value of 108°. On the other hand, test calculations on a symmetrical $Ru_6(CO)_{18}$ model, assuming a regular pentagonal pyramid with Ru−Ru = 2.80 Å, indicate a unique 88-CVE (8-SEP) favored electron count in agreement with the PSEPT.[20] Assuming a formal charge of −3 for the isolated CCCCH ligand, i.e. a formal C(16)−C(17) (weak) double bond and three σ lone pairs on the two atoms, the net electron transfer to the hexanuclear framework is computed to be 2.56 electrons. This electron donation comes essentially from the σ nonbonding and π-bonding orbitals (2.68 electron), while back-donation of 0.53 electrons occurs into the vacant π-antibonding levels. The C(16)−C(17) overlap population in the free $[CCCCH]^{3-}$ ligand is 1.019, a value barely larger than the corresponding value computed for **6a′** (0.920). This result indicates no significant participation of the C(16)−C(17) σ-bonding pair in the Ru_6 framework. Clearly, the pentagonal-pyramidal description does not appear valid for the distorted skeleton of **6a**.

The best starting point for understanding the electronic structure of cluster **6a′** is to analyze the framework as resulting from the interaction of the 66-CVE (7 SEP) $[Ru_4(CO)_{11}(CCCCH)]^{3-}$ octahedron with an $[Ru_2(CO)_4(PH_2)]^{3+}$ capping unit. The MO diagram of the former is shown on the left side of Figure 8. As previously mentioned, this diagram suggests that the 64-CVE count would be more favored for the isolated octahedron than the 66-CVE one for which the HOMO/LUMO gap is smaller. However, this contradicts the fact that many 66-CVE M_4E_2 octahedral clusters exist, in particular $M_4(\mu_4$-alkyne) compounds.[28] In agreement with the PSEPT, the MO diagrams for these molecules exhibit a single and large gap favoring the actual electron count.[28] Calculations on the $Fe_4(CO)_{12}(\mu_4\text{-}C_2H_2)$ model lead to a HOMO/LUMO gap of 1.90 eV. When one proton is removed from a carbon atom of this model, a high-lying lone pair is generated on the "bare" carbon atom, which becomes the HOMO, situated 0.63 eV above the next occupied level and 1.27 eV below the LUMO. A similar but magnified situation occurs in the $[Ru_4(CO)_{11}(CCCCH)]^{3-}$ octahedron. The HOMO can be described as being essentially a lone pair on the "bare" C(16) atom. It lies at −10.47 eV, a value close to the 2p AO energy of carbon, and is weakly antibonding with respect to all of the contacts involving C(16), especially C(16)−Ru(6).

The frontier orbital diagram of the $[Ru_2(CO)_4(PH_2)]^{3+}$ fragment is shown on the right side of Figure 8. It may be analyzed as resulting from the assembly of two weakly interacting d^6 ML_3 units. A typical isolated ML_3 system presents a block of three low-lying levels (the "t_{2g}" levels) situated below two hybridized d_π/p_π orbitals.[29] In the $[Ru_2(CO)_4(PH_2)]^{3+}$ "dimer", each "monomer" level generates a pair of in-phase and out-of-phase combinations. The six resulting "t_{2g}" combinations constitute a compact block of nonbonding levels lying below the four combinations of the d_π/p_π hybrids. Among these 10 d-type levels, none can be identified as being the real σ_{Ru-Ru} or σ^*_{Ru-Ru} orbital. If a localized two-electron Ru−Ru bond was present in the dinuclear bridge, one would expect that two of the t_{2g} orbitals would be Ru−Ru bonding and antibonding, respectively, preserving the hybrid combinations free for interacting with the octahedron. In such a situation, the Ru−Ru antibonding level would be too high in energy to be occupied, leaving only five low-lying d-type orbitals. In fact, the level which carries the largest Ru−Ru bonding character is the lowest hybrid combination, which has a π_σ bonding character (Figure 8). Although this orbital is vacant in $[Ru_2(CO)_4(PH_2)]^{3+}$, the computed total Ru−Ru overlap population (+0.057) indicates some weak bonding character. This is mainly due to through-bond interactions via the phosphido bridge.

One of the major interactions between this dinuclear unit and the $[Ru_4(CO)_{11}(CCCCH)]^{3-}$ octahedron occurs between the HOMO of the octahedron and the LUMO of the dinuclear bridge (Figure 8). The resulting bonding combination is occupied in **6a′**, leading to a significant occupation of the bridge LUMO in the cluster (0.89 electron). As a consequence, the Ru−Ru overlap population of the dinuclear fragment increases to +0.100 when bridging the octahedron. From this result it is clear that **6a** can be adequately described as a regular 66-CVE (7-SEP) Ru_4C_2 octahedron bicapped by a dinuclear unit with no localized σ-bond (24 electrons). From this point of view, the two "extra" electrons can be associated with the Ru(1)−Ru(2) system. It is likely that this peculiar situation is favored by the existence of the PR_2 bridge which helps keep the metal atoms proximate and induces through-bond interaction. It is also noteworthy that the HOMO of the 66-CVE octahedron, which is the lone pair on C(16), is strongly involved in the bonding with the bridge (its occupation in **6a′** is 1.10 electron).

Finally, we would like to make some comments on the electron-counting rules arising from the condensation principle.[20c,d] The demonstration of these rules is based on the description of a (n + m) vertex system as resulting from the interaction of two fragments of n and m vertexes, each behaving as a ligand toward the other. It has been shown that the CVE count of the overall system is the sum of the favored electron counts of the isolated fragments, minus twice the number of the two-orbital interactions between the two fragments.[20d] Our partitioning of **6a′** between the $[Ru_4(CO)_{11}(CCCCH)]^{3-}$ octahedron and the $[Ru_2(CO)_4(PH_2)]^{3+}$ bridging unit indicates that the five lowest (of the six) frontier orbitals of the dinuclear bridge lead to significant interaction with the other part of **6a′**. The only orbital which does

(28) Kahial, S.; Halet, J.-F.; Saillard, J.-Y. *New J. Chem.* **1991**, *15*, 843.

(29) Hoffmann, R. *Angew. Chem., Int. Ed. Engl.* **1982**, *21*, 711.

not participate in the bonding can be identified as being σ^*_{Ru-Ru}. Therefore, the 90-CVE count of **6a** can be obtained by adding 66 (favored electron count of an M_4C_2 octahedron) to 34 (favored electron count for an M−M unit) and subtracting 10 electrons corresponding to the creation upon interaction of five nonaccessible antibonding combinations. This peculiar situation (five major orbital interactions in the place of the expected six) arises from the fact that two capped faces of the octahedron are not orbital independent, since they share an edge. They form a Ru_3C rhombus which cannot offer more than five frontier orbitals suited for interacting with capping entities. This is why a naive application of the condensation rules, as well as of the capping principle, does not apply (*vide supra*). They both implicitly assume that the six frontier orbitals are associated with the two capped triangular faces.[20d] In fact, the 88-CVE values calculated from the fused polyhedra derivation and from the bicapped octahedron derivation (*vide supra*) have to be increased by 2, due to the existence of an extra nonbonding orbital.

Experimental Section

General Procedures. All manipulations and reactions were carried out under an atmosphere of dinitrogen using standard Schlenk-line techniques or in a drybox. Solvents for reactions, chromatography, and crystallizations were distilled under nitrogen from the appropriate drying agents prior to use. Reactions were monitored by thin-layer chromatography (Baker-flex IB2-F) and infrared spectroscopy (carbonyl region). Purification of products was performed by column chromatography using oven-dried (150 °C, 24 h) silica gel (70−230 mesh) on a dry-packed column or by thin-layer chromatography (TLC). Triruthenium dodecacarbonyl was purchased from Strem and used without further purification. The series of phosphino−butadiynes $Ph_2PC{\equiv}C{-}C{\equiv}CR$ (R = Bu^t, Ph, $SiMe_3$) was prepared according to the literature procedure.[8]

IR spectra were recorded on Nicolet 520 FTIR and Bio-Rad FTS-40A instruments, using sodium chloride cells of 0.5 mm path length for solution spectra (*n*-hexane or CH_2Cl_2). NMR spectra were recorded on Bruker AC 200, AM 200 (^{1}H, 200 MHz; $^{31}P\{^1H\}$ 81.0 MHz; $^{13}C\{^1H\}$ 50.3 MHz), and MSL 300 (^{1}H, 300 MHz; $^{31}P\{^1H\}$ 121.5 MHz) instruments. The $^{31}P\{^1H\}$ spectra are referenced externally to 85% H_3PO_4, and ^{1}H and ^{13}C are referenced to TMS via solvent shifts. Elemental analyses were performed by M−H−W Laboratories, Phoenix, AZ, and by the Microanalysis Service of the Institute for Biological Sciences, NRC, Ottawa.

EHMO Calculations: Computational Details. All calculations were carried out within the extended Huckel method[30] using the modified Wolfsberg−Helmholz formula.[31] Standard atomic parameters were taken for H, C, O, and P. The exponent (ζ) and the valence shell ionization potential (H_{ii} in eV) for Ru were, respectively, 2.078, −8.60 for 5s, 2.043, −5.10 for 5p. The H_{ii} value for 4d was set to −12.20. A linear combination of two Slater-type orbitals ($\zeta_1 = 5.378$, $c_1 = 0.5340$; $\zeta_2 = 2.203$, $c_2 = 0.6365$) was used to represent the atomic 4d orbitals. To avoid oversimplifications and steric problems arising from a symmetry idealization of **6a** (which is only of rough C_s symmetry), the unmodified experimental X-ray structure was used. The model **6a′** was then generated by replacing the phenyl groups on the phosphorus atom and the terminal CMe_3 of the C_4Bu^t ligand by hydrogen atoms. In this process, the experimental valence angles were kept unchanged and the following bond distances (A) were assumed: P−H 1.42 Å; C−H = 1.09 Å.

Synthesis of $Ru_4(CO)_9(\mu\text{-}PPh_2)_2\{\mu_4\text{-}\eta^1,\eta^2,\eta^2,\eta^1\text{-}C{\equiv}C{-}C{=}C(Bu^t)\text{-}C{\equiv}C{-}C{\equiv}CBu^t\}$ (2), $Ru_4(CO)_{10}(\mu\text{-}CO)(\mu_4\text{-}PPh)\{\mu_4\text{-}\eta^1,\eta^1,\eta^2,\eta^2\text{-}(Bu^tC{\equiv}C)C{\equiv}CPh\}$ (3), $Ru_4(CO)_{10}(\mu_4\text{-}PPh)(\mu_4\text{-}\eta^1,\eta^1,\eta^3,\eta^3\text{-}PhC{\equiv}C{-}C{\equiv}CBu^t)$ (4), $Ru_5(CO)_{11}(\mu\text{-}CO)(\mu\text{-}PPh_2)_2(\mu_3\text{-}\eta^1,\eta^1,\eta^1\text{-}C{\equiv}C{-}C{\equiv}CBu^t)(\mu_4\text{-}C)$ $(\mu_2\text{-}\eta^1,\eta^1\text{-}C{-}C{\equiv}CBu^t)$ (5) and $Ru_6(CO)_{13}(\mu\text{-}CO)_2(\mu\text{-}PPh_2)(\mu_5\text{-}C)(\mu_3\text{-}\eta^1,\eta^1,\eta^1\text{-}C{-}C{\equiv}CBu^t)$ (6a). Triruthenium dodecacarbonyl (2.50 g, 3.91 mmol) was dissolved in tetrahydrofuran (300 mL, 3 freeze−pump−thaw cycles) and treated with a slight excess of $Ph_2PC{\equiv}C{-}C{\equiv}CBu^t$ (1.20 g, 4.13 mmol). A few drops of sodium benzophenone ketyl catalyst in THF was added, causing an immediate color change to deep red. After the mixture was stirred for 10 min, IR (2098 w, 2047 s, 2031 ms, 2016 s cm^{-1}) indicated the complete consumption of $Ru_3(CO)_{12}$ while a spot TLC showed a single red-orange band that we assign as the monosubstituted species $Ru_3(CO)_{11}(Ph_2PC{\equiv}C{-}C{\equiv}CBu^t)$. The solution was then set to reflux for 4 h, causing a considerable darkening. On cooling, the solvent was partially evaporated *in vacuo* and the residue absorbed onto a small amount of silica gel. Column chromatography on silica yielded a minor band of $Ru_3(CO)_{12}$ (identified by IR), using *n*-hexane as eluant, followed by a broad pale yellow zone of **1a** (805 mg, 31%), eluted with CH_2Cl_2−*n*-hexane (1:49). Increasing the polarity of the solvent allowed the successive elution of orange (CH_2Cl_2−*n*-hexane (1:19), **4**, 110 mg, 3%), red-brown (CH_2Cl_2−*n*-hexane (1:9), **6a**, 162 mg, 3%), orange (CH_2Cl_2−*n*-hexane (1:6), **3** + **5**), and green-blue (CH_2Cl_2−*n*-hexane (1:4), **2**, 290 mg, 12%) bands. Further purification of each was effected by TLC, which allowed the resolution of **3** and **5** into two separate orange bands (yields 42 mg, 1% and 148 mg, 5%, respectively).

Crystals of **2**−**6** suitable for X-ray diffraction analysis were grown from the following solvent systems: **2**, green needles grown from CH_2Cl_2/MeOH at room temperature; **3**, red prisms grown from *n*-hexane at −20 °C; **4**, red-orange plates from *n*-hexane at −20 °C; **5**, dark orange plates grown from diethyl ether/*n*-hexane at room temperature; **6a**, dark red-brown prisms grown from Et_2O/*n*-hexane at −20 °C.

2: IR (*n*-C_6H_{14}) ν(CO)/cm^{-1} 2079 ms, 2038 s, 2022 ms, 2012 vs, 2002 w, 1991 mw, 1966 mw; ^{1}H NMR ($CDCl_3$) δ 7.58−7.17 (m, 20H, Ph), 1.19 (s, 9H, Bu^t), 1.13 (s, 9H, Bu^t); ^{31}P NMR ($CDCl_3$, 298 K) δ 209.2 (s); ^{31}P NMR (CD_2Cl_2, 183 K) δ 211.7 (s). Anal. Calcd for $C_{49}H_{38}O_9P_2Ru_4$: C, 47.58; H, 3.10. Found: C, 47.75; H, 3.09. Mp > 400 °C.

3: IR (*n*-C_6H_{14}) ν(CO)/cm^{-1} 2086 mw, 2054 vs, 2036 s, 2028 s, 2004 m, 1983 mw, 1846 w br; ^{1}H NMR ($CDCl_3$) δ 7.21−6.18 (m, 10H, Ph), 0.69 (s, 9H, Bu^t); $^{13}C\{^1H\}$ ($CDCl_3$) δ 200.8 (d, J_{PC} = 12 Hz, CO), 145.7 (s, C diyne), 145.6 (s, CC_{ipso}), 133.6 (d, J_{PC} = 31 Hz, PC_{ipso}), 130.8−124.8 (m, Ph), 117.8 (s, C diyne), 110.9 (s, C diyne), 77.2 (s, C diyne), 29.7 (s, CMe_3), 29.5 (s, CMe_3); ^{31}P NMR ($CDCl_3$) δ 251.5 (s). Anal. Calcd for $C_{31}H_{19}O_{11}PRu_4$: C, 37.13; H, 1.91. Found: C, 37.29; H, 2.10. Mp 151 °C.

4: IR (*n*-C_6H_{14}) ν(CO)/cm^{-1} 2082 w, 2059 vs, 2025 s, 2021 s, 2010 m, 1968 m; ^{1}H NMR ($CDCl_3$) δ 7.61−6.98 (m, 10H, Ph), 1.78 (s, 9H, Bu^t); $^{13}C\{^1H\}$ (C_6D_6) δ 204.3 (d, J_{PC} = 8 Hz, C diyne), 194.7 (d, J_{PC} = 9 Hz, CO), 193.5 (d, J_{PC} = 40 Hz, C diyne), 154.4 (d, J_{PC} = 11 Hz, C diyne), 146.5 (s, CC_{ipso}), 142.4 (d, J_{PC} = 23 Hz, PC_{ipso}), 133.3−125.8 (m, Ph), 37.6 (s, CMe_3), 36.0 (s, CMe_3); ^{31}P NMR ($CDCl_3$) δ 446.0 (s). Anal. Calcd for $C_{30}H_{19}O_{10}PRu_4$: C, 36.97; H, 1.96. Found: C, 36.92; H, 1.92. Mp 229 °C.

5: IR (*n*-C_6H_{14}) ν(CO)/cm^{-1} 2086 w, 2045 w, 2032 m, 2019 s, 2015 sh, 1981 mw br; ^{1}H NMR ($CDCl_3$) δ 7.79−7.27 (m, 20H, Ph), 1.10 (s, 9H, Bu^t), 1.04 (s, 9H, Bu^t); $^{13}C\{^1H\}$ ($CDCl_3$) δ 294.5 (d, J_{PC} = 16 Hz, C diyne), 202.1 (s, CO), 200.8 (s, CO), 199.2 (d, J_{PC} = 8 Hz, CO), 198.1 (d, J_{PC} = 8 Hz, CO), 196.8 (d, J_{PC} = 6 Hz, CO), 195.7 (d, J_{PC} = 11 Hz, CO), 194.5 (d, J_{PC} = 9 Hz, CO), 194.1 (d, J_{PC} = 8 Hz, CO), 187.3, (s, CO), 185.5 (s, C

(30) (a) Hoffmann, R. *J. Chem. Phys.* **1963**, *39*, 1397. (b) Hoffmann, R.; Lipscomb, W. N. *J. Chem. Phys.* **1962**, *36*, 2179.
(31) Ammeter, J. H.; Burgel, H.-B.; Thibeault, J. C.; Hoffmann, R. *J. Am. Chem. Soc.* **1978**, *100*, 3686.

diyne), 158.1 (d, J_{PC} = 3 Hz, C diyne), 142.9 (d, J_{PC} = 32 Hz, PC_{ipso}), 142.6 (d, J_{PC} = 24 Hz, PC_{ipso}), 140.3 (d, J_{PC} = 24 Hz, PC_{ipso}), 137.6 (d, J_{PC} = 35 Hz, PC_{ipso}), 133.8−127.4 (m, Ph), 105.3 (s, C diyne), 94.8 (s, C diyne), 91.3 (s, C diyne), 72.4 (d, J_{PC} = 9 Hz, C diyne), 62.5 (d, J_{PC} = 3 Hz, C diyne), 30.2 (s, C*Me*$_3$), 29.9 (s, C*Me*$_3$), 28.6 (s, *C*Me$_3$), 28.2 (s, *C*Me$_3$); ^{31}P NMR ($CDCl_3$) δ 209.6 (s, closed μ-PPh_2), 54.7 (s, open μ-PPh_2). Anal. Calcd for $C_{52}H_{38}O_{12}P_2Ru_5$: C, 43.92; H, 2.69. Found: C, 44.11; H, 2.80. Mp 191 °C.

6a: IR (CH_2Cl_2) ν(CO)/cm^{-1} 2080 w, 2049 m, 2041 vs, 2019 s, 1872 w br; ^{1}H NMR ($CDCl_3$) δ 7.82−7.40 (m, 10H, Ph), 1.10 (s, 9H, Bu^t); ^{13}C{^{1}H} (THF-d_8) δ 302.7 (d, J_{PC} = 6 Hz, C_α), 218.6 (s, μ-CO), 204.2 (d, J_{PC} = 4 Hz, CO), 200.6 (s, CO), 197.9 (s, CO), 197.1 (d, J_{PC} = 6 Hz, CO), 185.2 (s, C_β), 137.9 (d, J_{PC} = 44 Hz, PC_{ipso}), 136.0−129.8 (m, Ph), 126.0 (s, C_δ), 98.9 (s, C_γ), 31.0 (s, C*Me*$_3$), 30.2 (s, *C*Me$_3$); ^{31}P NMR ($CDCl_3$) δ 251.6 (s). Anal. Calcd for $C_{35}H_{19}O_{15}PRu_6$: C, 31.92; H, 1.45. Found: C, 31.85; H, 1.56. Mp 134 °C.

Synthesis of $Ru_6(CO)_{13}(\mu$-$CO)_2(\mu$-$PPh_2)(\mu_5$-$C)(\mu_3$-η^1,η^1,η^1-C−C≡CPh) (6b). A similar procedure to that described for **6a** was followed using $Ru_3(CO)_{12}$ (2.0 g, 3.13 mmol) and Ph_2-PC≡C−C≡CPh (1.10 g, 3.54 mmol) with refluxing for 2.5 h. Column chromatography on silica yielded a minor band of Ru_3-$(CO)_{12}$ (identified by IR) using *n*-hexane as eluant, followed by a broad pale yellow zone of $Ru_2(CO)_6(\mu$-$PPh_2)(\mu$-η^1,η^2-C≡C−C≡CPh) (**1b**; 504 mg, 24%) eluted with CH_2Cl_2−*n*-hexane (1:49). After an unidentified orange band, red-brown **6b** was isolated using CH_2Cl_2−*n*-hexane (1:9) as eluant. Further purification by TLC yielded **6b** as a red-brown powdery solid (53 mg, 1%). An analytically pure sample was crystallized from diethyl ether/hexane at −20 °C.

6b: IR (CH_2Cl_2) ν(CO)/cm^{-1} 2080 w, 2050 m, 2042 vs, 2020 s, 1873 w br; ^{1}H NMR ($CDCl_3$) δ 7.86−6.60 (m, 10H, Ph); ^{13}C-{^{1}H} ($CDCl_3$) δ 302.8 (d, J_{PC} = 6 Hz, C_α), 213.5 (s, μ-CO), 203.0 (d, J_{PC} = 4 Hz, CO), 199.2 (s, CO), 196.4 (s, CO), 195.9 (d, J_{PC} = 6 Hz, CO), 183.9 (s, C_β), 137.5−126.8 (m, Ph), 123.2 (s, C_δ), 111.2 (s, C_γ); ^{31}P NMR ($CDCl_3$) δ 253.1 (s). Anal. Calcd for $C_{37}H_{15}O_{15}PRu_6$: C, 33.24; H, 1.13. Found: C, 33.42; H, 1.39. Mp > 260 °C.

Synthesis of $\{Ru_2(CO)_6(\mu$-$PPh_2\}_2(\mu$-η^1,η^2:μ-η^1,η^2-C≡C−C≡C−) (7). A similar procedure to that described for **1a** was followed using $Ru_3(CO)_{12}$ (2.0 g, 3.13 mmol) and Ph_2PC≡C−C≡C$SiMe_3$ (1.10 g, 3.59 mmol) with refluxing for 2 h. Column chromatography on silica yielded a minor band of $Ru_3(CO)_{12}$ (identified by IR) using *n*-hexane as eluant, followed by a broad yellow zone of $Ru_2(CO)_6(\mu$-$PPh_2)(\mu$-η^1,η^2-C≡C−C≡C$SiMe_3$) (**1c**; 414 mg, 20%) eluted with CH_2Cl_2−*n*-hexane (1:49). A broad bright orange band of **7** was then obtained using CH_2Cl_2−*n*-hexane (1:19), which yielded a yellow-orange microcrystalline solid on evaporation of the solvent. Yield: 246 mg, 14%. The crystal used for X-ray analysis was grown from heptane−toluene (4:1) at −20 °C.

7: IR (*n*-C_6H_{14}) ν(CO)/cm^{-1} 2089 m, 2081 s, 2059 s, 2024 s, 2012 m, 2001 s, 1992 mw; ^{1}H NMR ($CDCl_3$) δ 7.54−7.17 (m, Ph); ^{13}C{^{1}H} ($CDCl_3$) δ 197.2 (d, J_{PC} = 12 Hz, CO), 194.5 (d, J_{PC} = 72 Hz, CO), 193.4 (d, J_{PC} = 6 Hz, CO), 138.7 (d, J_{PC} = 30 Hz, PC_{ipso}), 133.1 (d, J_{PC} = 34 Hz, PC_{ipso}), 133.9−128.0 (m, Ph), 129.0 (d, J_{PC} = 12 Hz, C_β), 103.3 (d, J_{PC} = 27 Hz, C_α); ^{31}P NMR ($CDCl_3$) δ 121.8 (s). Anal. Calcd for $C_{20}H_{10}O_6PRu_2$: C, 41.46; H, 1.74. Found: C, 41.12; H, 1.76. Mp 166 °C.

Thermolysis of $Ru_4(CO)_{10}(\mu$-$CO)(\mu_4$-$PPh)\{\mu_4$-$\eta^1,\eta^1,\eta^2,\eta^2$-(Bu^{t}C≡C)C≡CPh} (3). A solution of $Ru_4(CO)_{10}(\mu$-$CO)(\mu_4$-$PPh)\{\mu_4$-$\eta^1,\eta^1,\eta^2,\eta^2$-(Bu^{t}C≡C)C≡CPh} (**3**) (20 mg, 0.020 mmol) in heptane (15 mL) was heated to reflux (100 °C), and the reaction was monitored by IR spectroscopy. After 30 min, the IR spectrum indicated complete conversion to complex **4**. Upon cooling to room temperature, the solvent was partially removed *in vacuo*. The remaining solution (2 mL) was passed through a 1 in. Pasteur pipet silica plug and an orange band eluted using heptane. On concentration of the solution and overnight cooling (−20 °C), red-orange crystals were obtained and identified by IR, comparative TLC, and melting point as Ru_4-$(CO)_{10}(\mu_4$-$PPh)(\mu_4$-$\eta^1,\eta^1,\eta^3,\eta^3$-PhC≡C−C≡CBu^t) **4** (18 mg, 93%).

Crystal Structure Determinations: 3, 4, 5, and 6a. Relevant crystallographic details are given in Table 1. Background measurements using the stationary crystal, stationary counter method were made at the beginning and end of each scan, each for 25% of the total scan time. Two standard reflections monitored every 100 reflections showed no significant changes during the data collection. Data were corrected for Lorentz and polarization effects and absorption (face-indexed numerical).

The structures were solved by Patterson and Fourier and refined by full-matrix least-squares first with isotropic thermal parameters and then with anisotropic thermal parameters for all non-hydrogen atoms. In the final cycles of refinement, hydrogen atoms were constrained to ideal positions with a riding model. In **5**, the Bu^t group, comprising carbon atoms C(26)−C(28), showed evidence of two-site disorder. A satisfactory (50:50 occupancy) model was refined for atoms C(25)/C(25A), C(27)/C(27A), and C(28)/C(28A) with atom C(26) being common to both models. H atoms were not included on these atoms. Computations were carried out on a MicroVAX II computer using the SHELXTL-PLUS program system.

2 and 7. Crystals of these clusters were thin plates that diffracted poorly. The diffraction peaks were broad and often split. The elevated final *R* values are due to the poor quality of the crystals. Full hemispheres of data were collected (1250, 0.3° − ω frames) and empirical absorption corrections applied. The merging *R* values for equivalent reflections after correction for absorption were 0.105 and 0.042 for **2** and **7**, respectively.

The structures were solved by direct methods and refined by full-matrix least squares. The hydrogen atoms were placed in calculated positions and allowed to ride on their parent atom. The phenyl ring in **7** comprised of atoms C(15)−C(20) was disordered over three sites. These were modeled as rigid groups with isotropic thermal parameters whose occupancies summed to unity (relative occupancies 0.46:0.28:0.26). Hydrogens on these carbons were placed in calculated positions for final refinement. Computations were performed on a Silicon Graphics INDY computer, using the NRCVAX suite of programs.[32] For all structures, the function minimized in the least-squares calculations was $\sum w(|F_o| - |F_c|)^2$. A weighting scheme of $w^{-1} = \sigma^2(F)$ was used.

Acknowledgment. We are grateful to the Natural Sciences and Engineering Research Council of Canada (NSERC) and the National Research Council of Canada for financial support of this work. We also thank the NSERC for a Canada International Fellowship Award to P.B. and a Canadian Government Laboratories Visiting Fellowship to P.J.L.

Supporting Information Available: Tables of refined and calculated atomic coordinates, anisotropic thermal parameters, and bond lengths and angles (49 pages). Ordering information is given on any current masthead page. Observed and calculated structure factors are available from the authors upon request.

OM9800593

(32) Gabe, E. J.; Le Page, Y.; Charland, J.-P.; Lee, F. L.; White, P. S. *J. Appl. Crystallogr.* **1989**, *22*, 384.